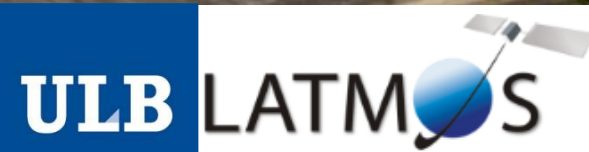


Measuring volcanic ash and windblown sand with IASI



Lieven Clarisse
P.-F. Coheur, J. Hadji-Lazaro and C. Clerbaux

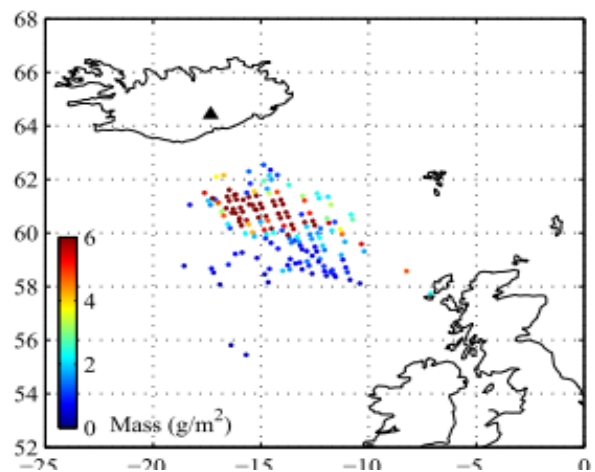
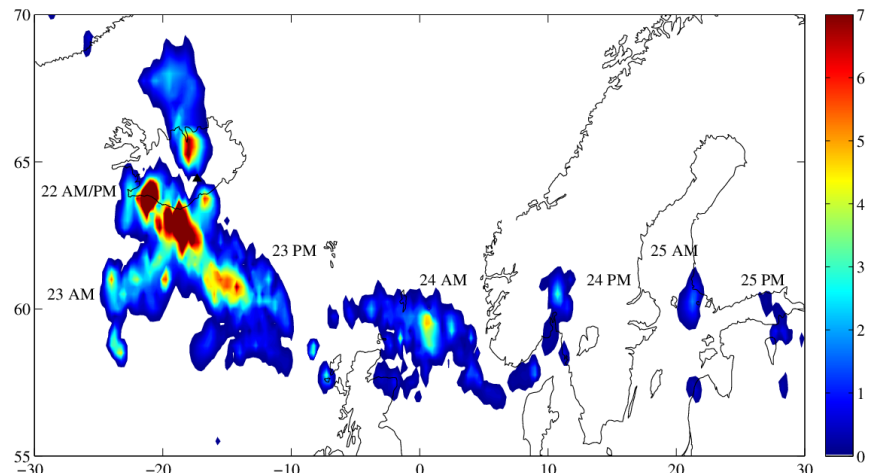


Lookup table approach

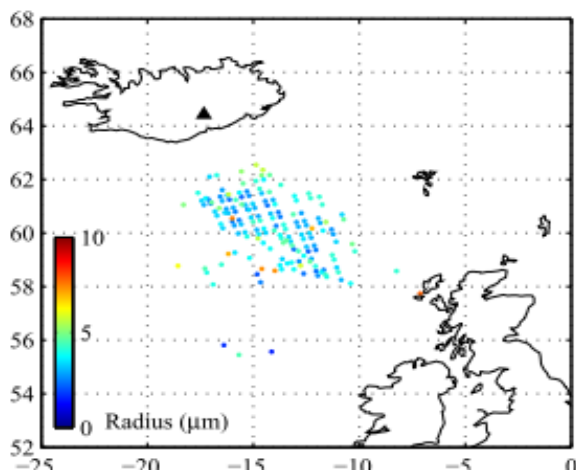
1. Database of forward simulations

2. Least mean square retrieval

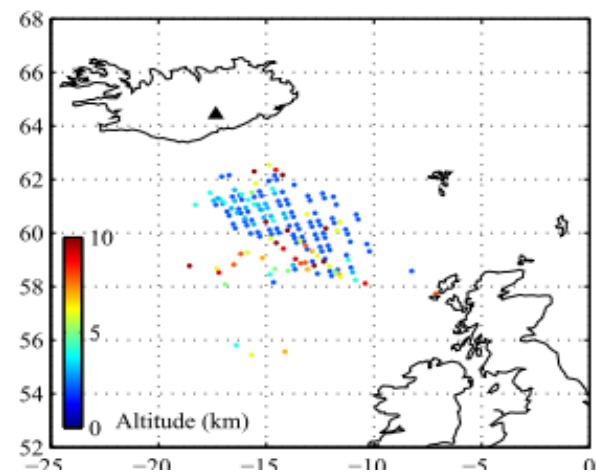
3. Optical depth masses, radius and altitude



OD/Mass

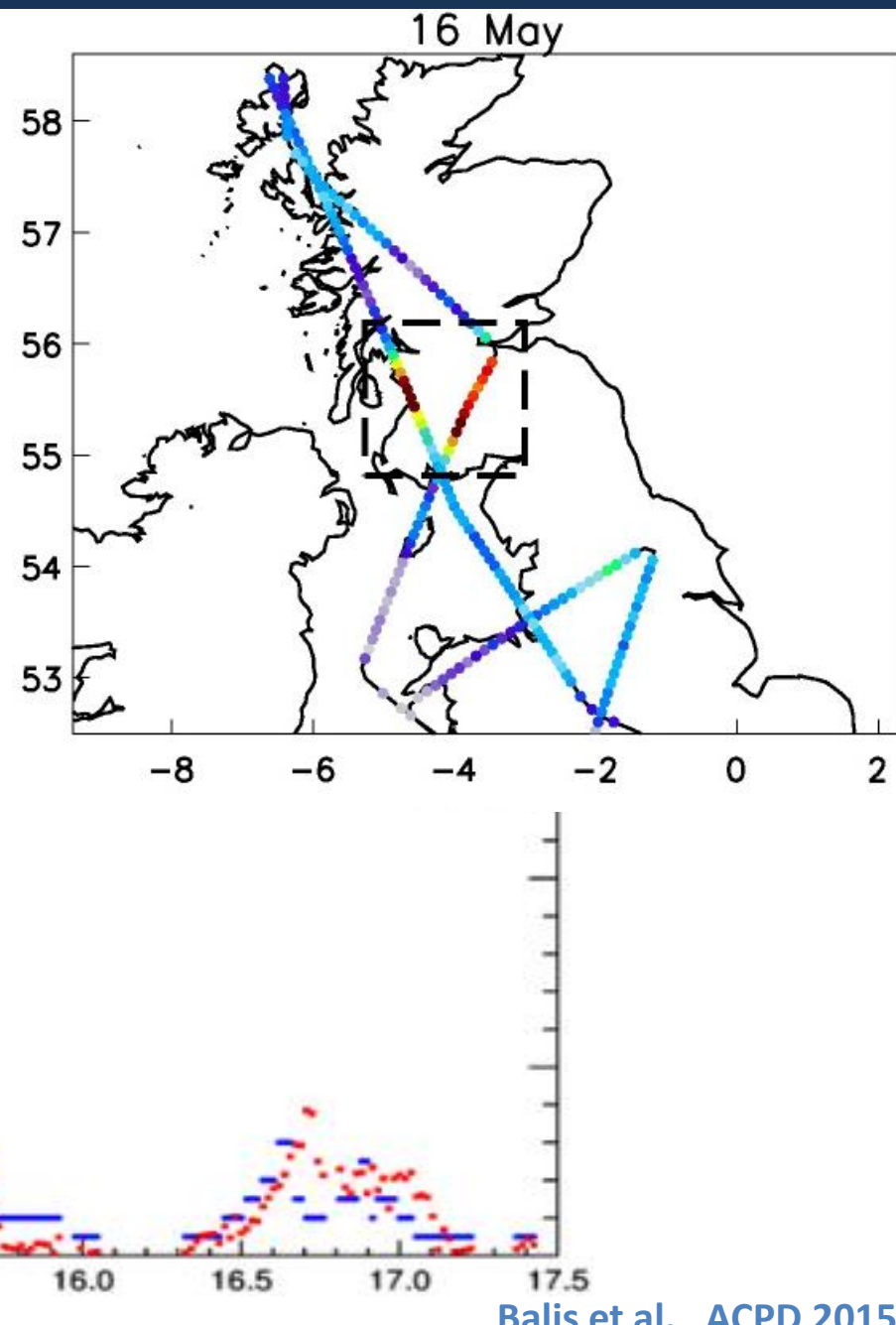
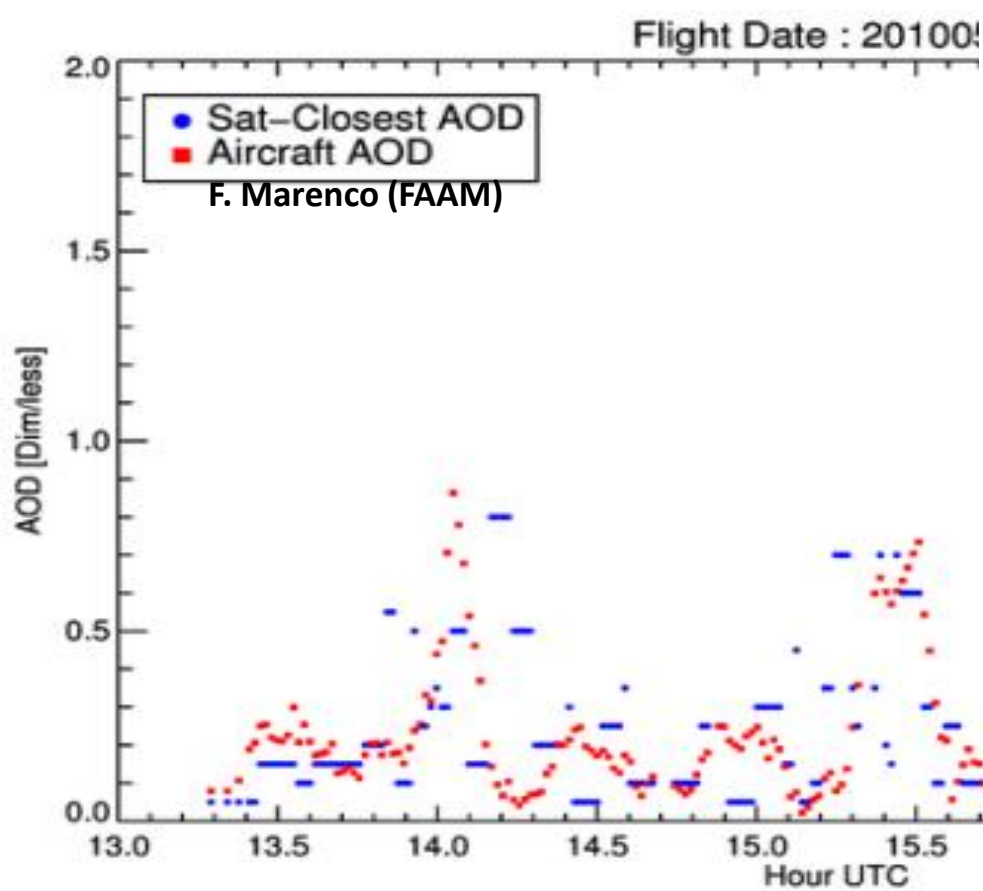


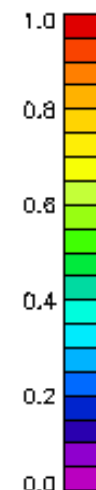
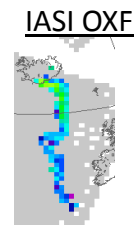
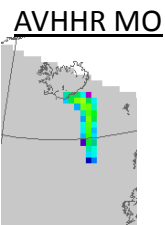
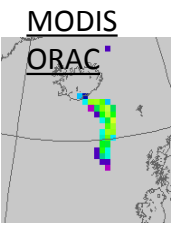
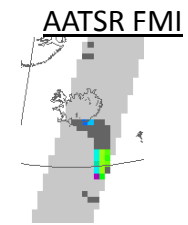
Radius



Altitude

Validation by
Laboratory of Atmospheric Physics
Aristotle University of Thessaloniki

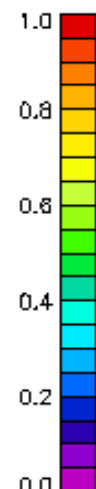
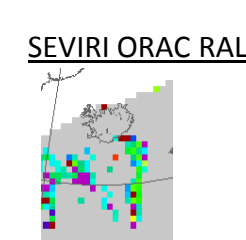
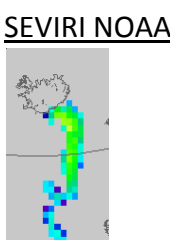
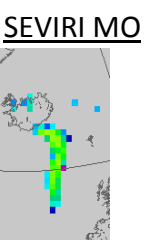
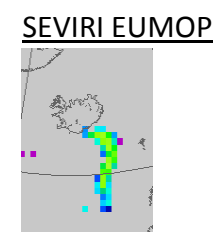
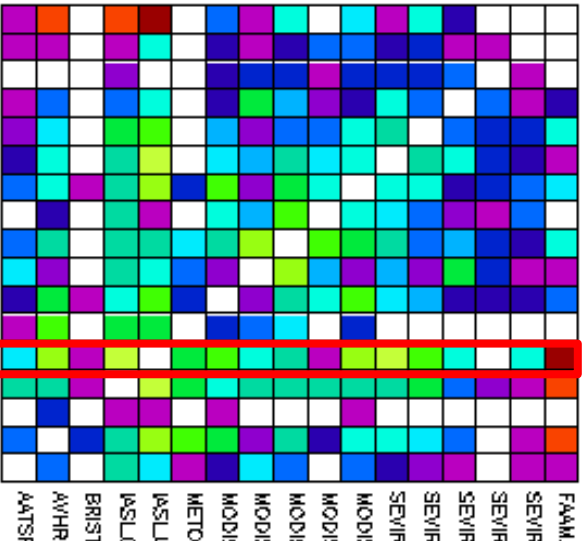




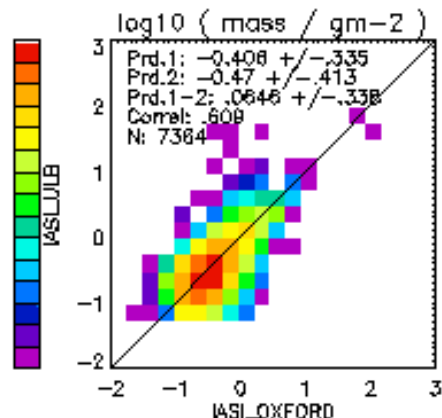
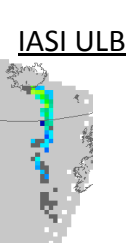
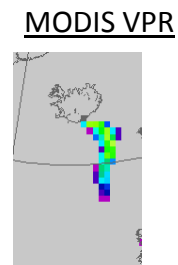
MASS

	AM_MO	SEVIRI_VADUGS	SEVIRLORAC_RAL	SEMRLLNOAA	SEMRLEUMOP	SEVIRI_MO	MODIS_VPR	MODIS_RAL	MODIS_ORAC	MODIS_NOAA	MODIS_LUT	METOP_PLANETA	IASI_ULB	IASLOXFORD	BRISTOL_JASI	AVHRR_MO	AATSR_FMI	FAAM
AM_MO	1.0																	
SEVIRI_VADUGS		1.0																
SEVIRLORAC_RAL			1.0															
SEMRLLNOAA				1.0														
SEMRLEUMOP					1.0													
SEVIRI_MO						1.0												
MODIS_VPR							1.0											
MODIS_RAL								1.0										
MODIS_ORAC									1.0									
MODIS_NOAA										1.0								
MODIS_LUT											1.0							
METOP_PLANETA												1.0						
IASI_ULB													1.0					
IASLOXFORD														1.0				
BRISTOL_JASI															1.0			
AVHRR_MO																1.0		
AATSR_FMI																	1.0	
FAAM																		1.0

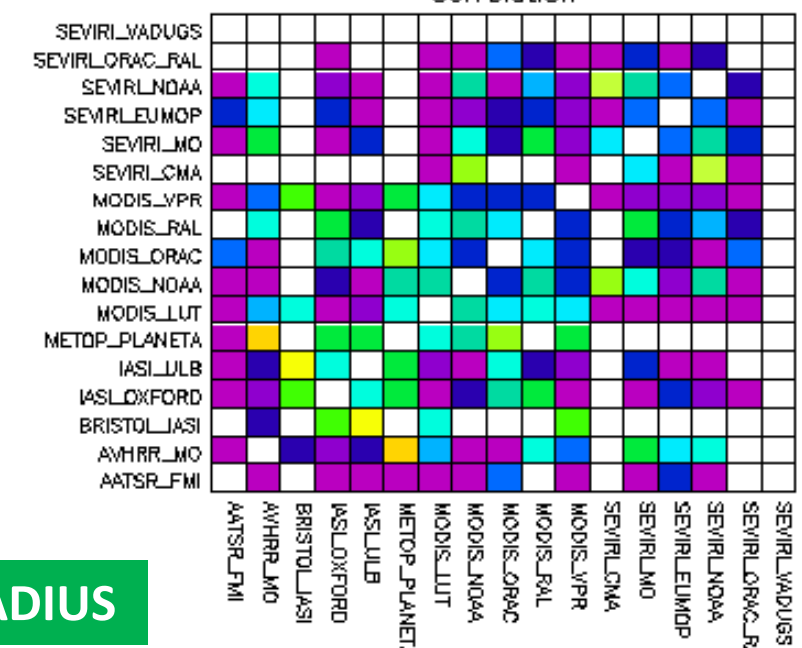
Correlation

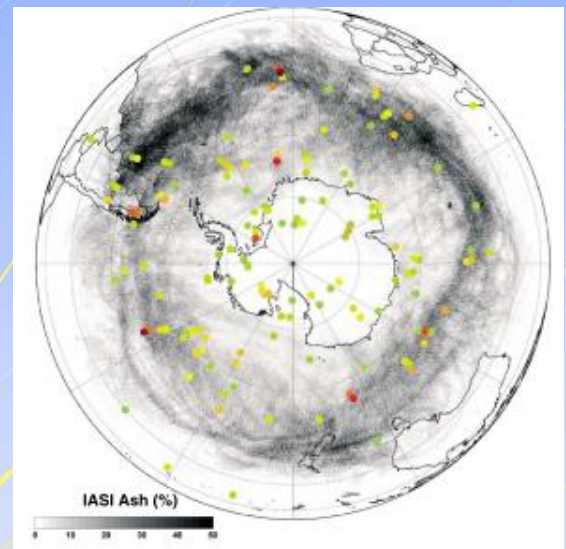
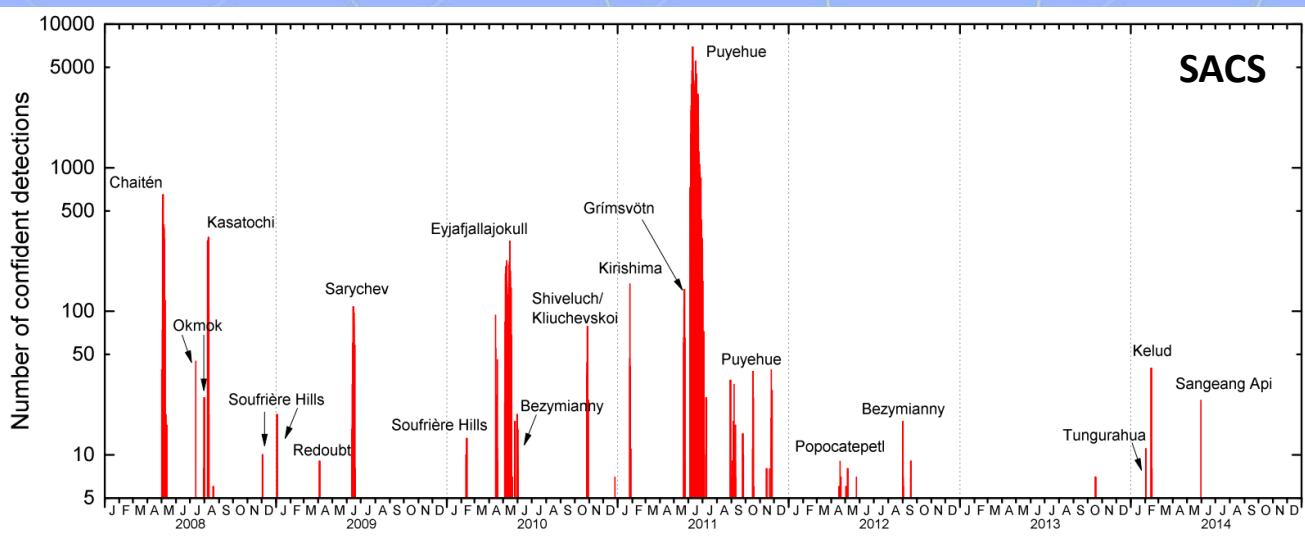


RADIUS



9.0510.0511.0512.0513.0514.0516.0517.0





Size distributions

Big grains go far: understanding the discrepancy between tephrochronology and satellite infrared measurements of volcanic ash

J. A. Stevenson¹, S. C. Millington², F. M. Beckett², G. T. Swindles³, and T. Thordarson⁴

Clouds

Ash and ice clouds during the Mt. Kelud Feb 2014 eruption as interpreted from IASI and AVHRR/3 observations

Arve Kylling¹

Exploiting hyperspectral sounders for volcanic ash remote sensing

Luke Western (1), Matthew Watson (1), and Peter Francis (2)

EGU

A model sensitivity study of the impact of clouds on satellite detection and retrieval of volcanic ash

A. Kylling¹, N. Kristiansen¹, A. Stohl¹, R. Buras-Schnell², C. Emde³, and J. Gasteiger³

CHAPTER

11

Infrared Sounding of Volcanic Ash

L. Clarisse, F. Prata

OUTLINE

1. Infrared Radiation and Volcanic Ash	190	<i>2.2 Hyperspectral</i>	202
1.1 Volcanic Aerosols and Trace Gases	190		
1.2 Forward Modeling	192	3. Retrieval Algorithms	204
1.3 Sensitivity Parameters	193	4. Validation	208
1.3.1 Composition and Particle Shape	193	<i>4.1 Instrument-to-Instrument Intercomparisons</i>	210
1.3.2 Loading and Altitude	195	<i>4.2 Verification Against Independent Observations</i>	211
1.3.3 Particle Size and Size Distribution	196	<i>4.3 Comparisons With Model Simulations</i>	213
1.3.4 Atmospheric and Surface Parameters	198		
1.4 Example Observations	198	5. Outlook	215
2. Ash Detection	200	Acknowledgments	215
2.1 Broadband	200		

Mackie, S. et. Al (Ed.) Volcanic ash: methods of observation and monitoring.
Elsevier, 2015

ULB neural network dust product



Inverse modelling in remote sensing

$$Y = \min_z G(F(x_z), \text{auxiliary parameters})$$

Minimization method

Minimization function

Minimization method

$x = F^{-1}(y)$

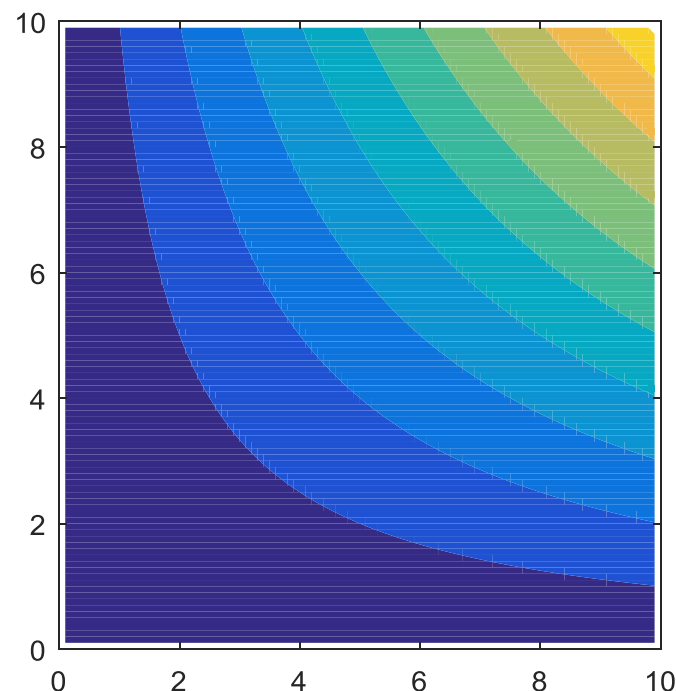
Newton/Gauss iteration

Look-up-table

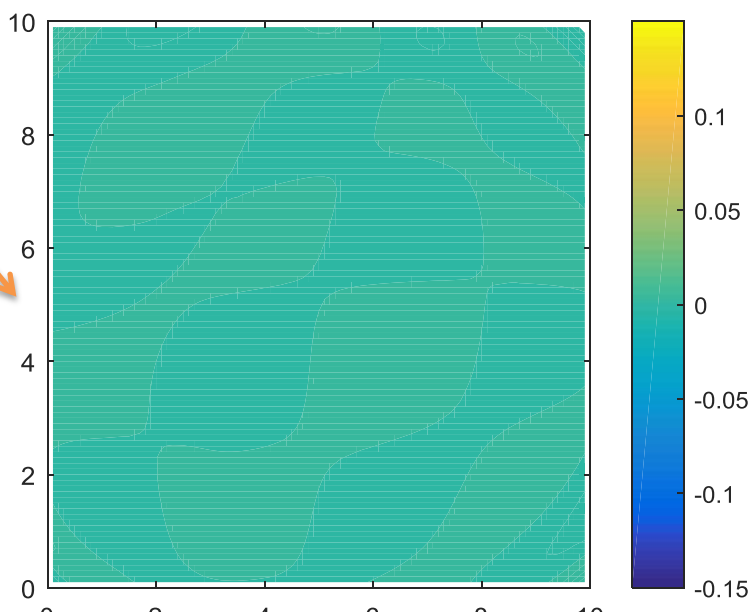
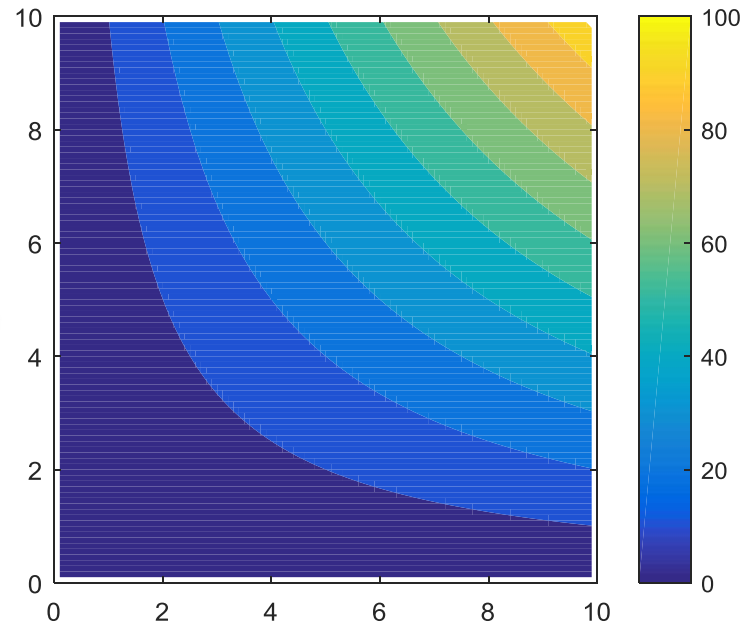
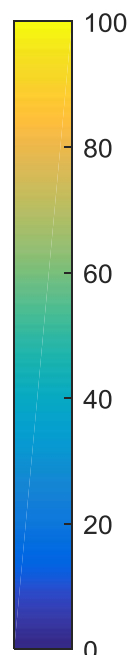
Neural network

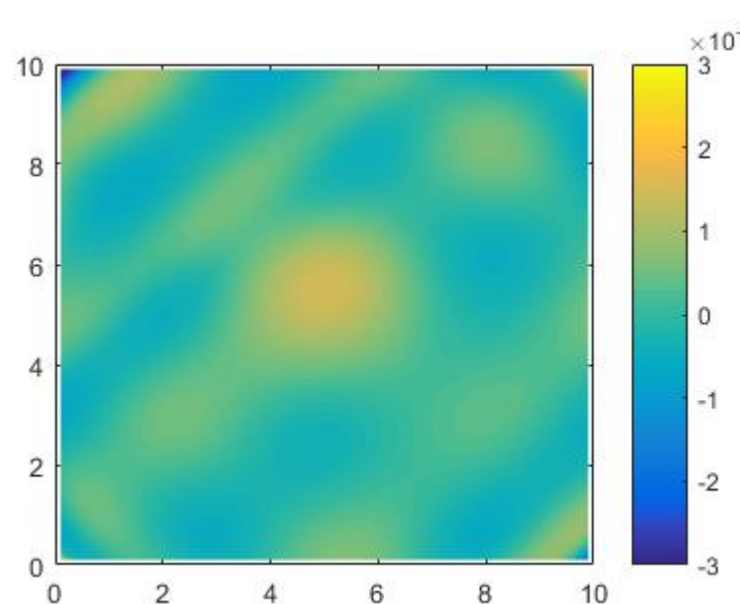
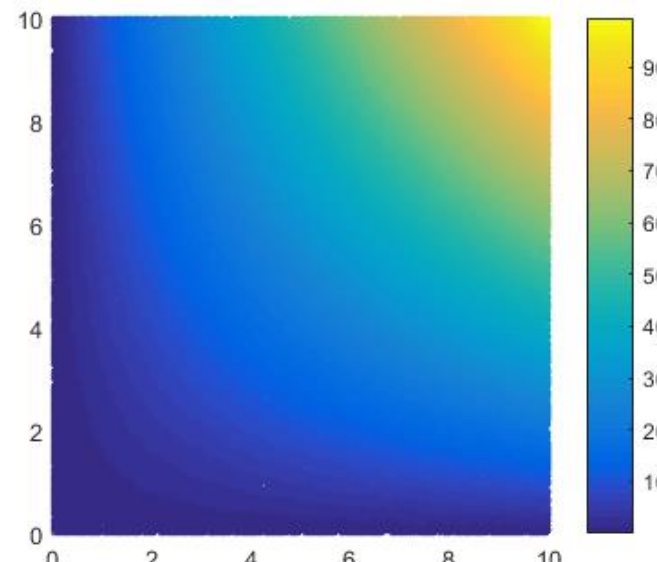
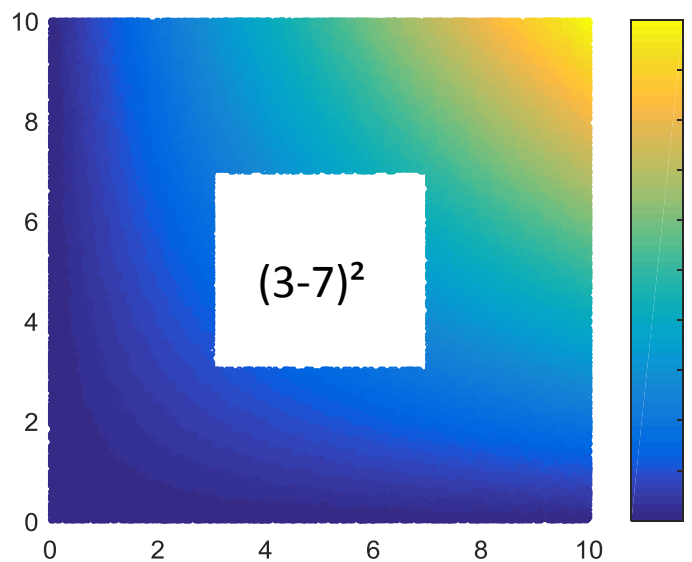
- Approximate any function to arbitrary accuracy
- Large input parameters space ($100 + \text{input parameters} = \text{no problem}$)
- Excellent interpolation capabilities

Training data



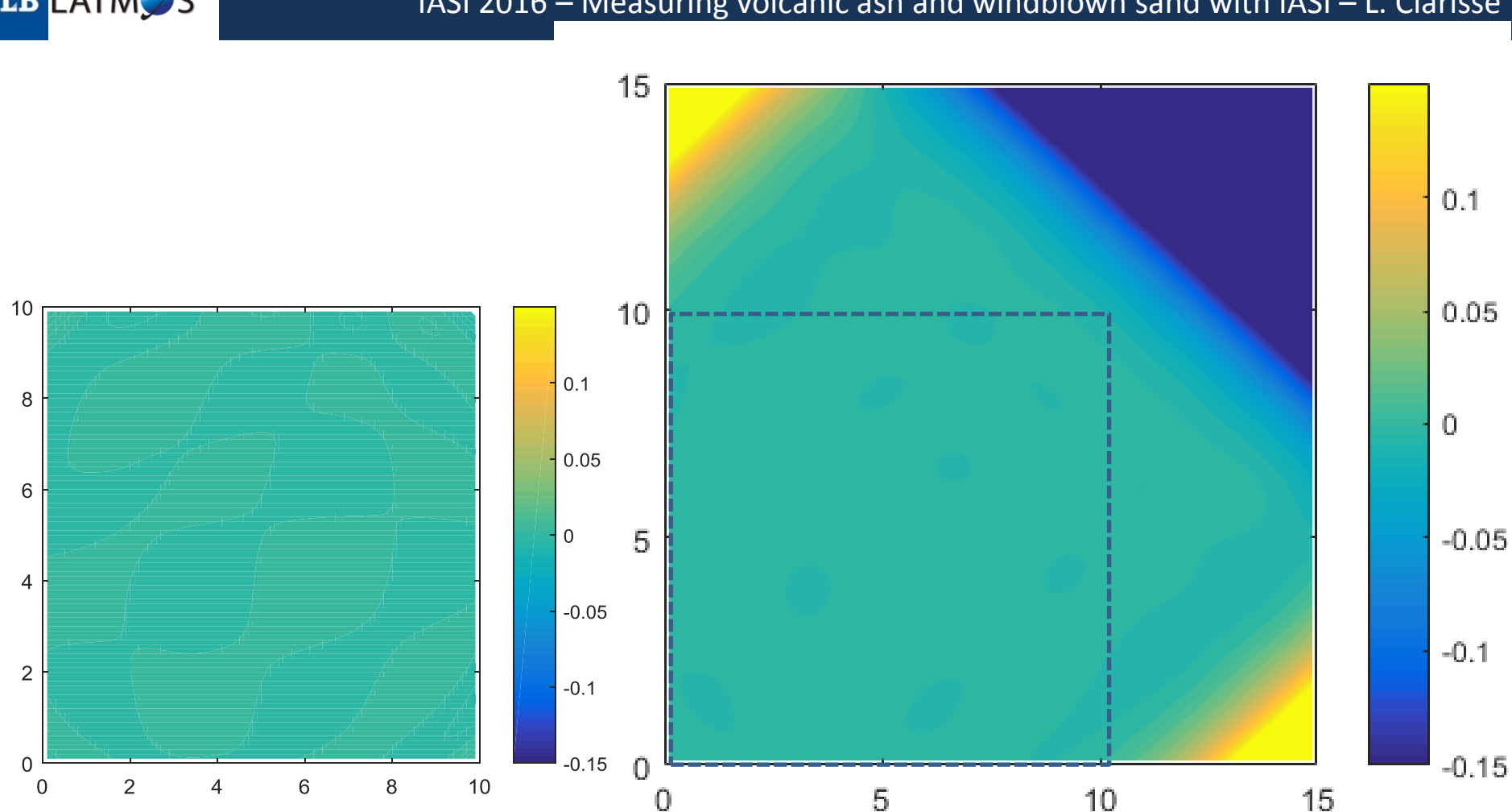
$$F(x,y) = x * y$$





$$F(x,y) = x * y$$

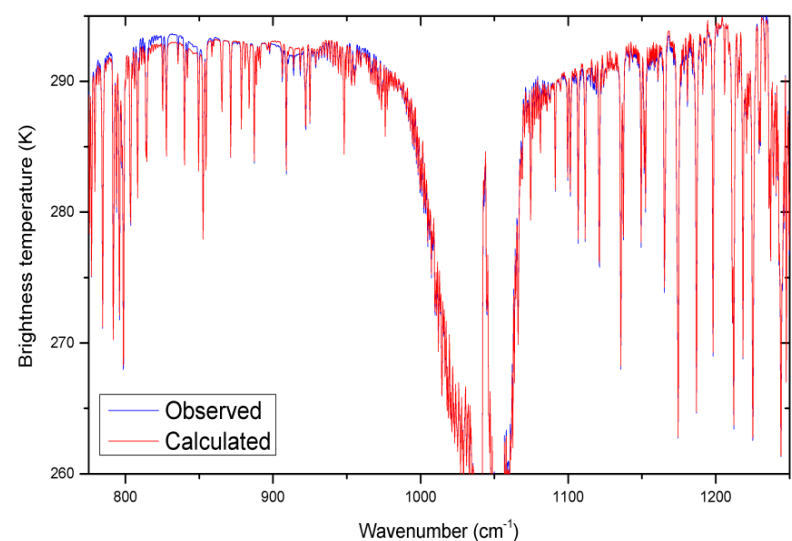
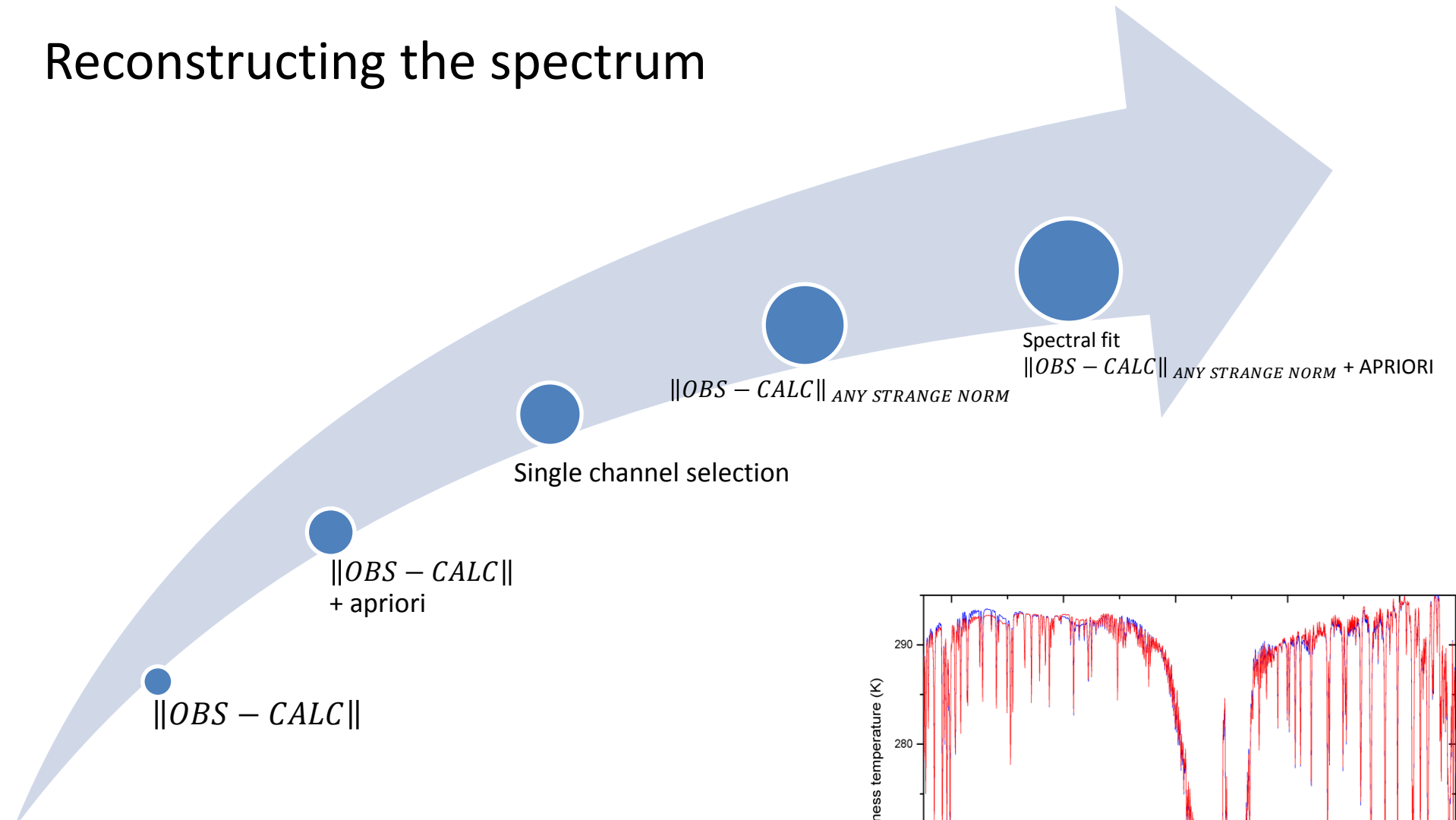
Free interpolation!!



Training data (input, output pair) should be

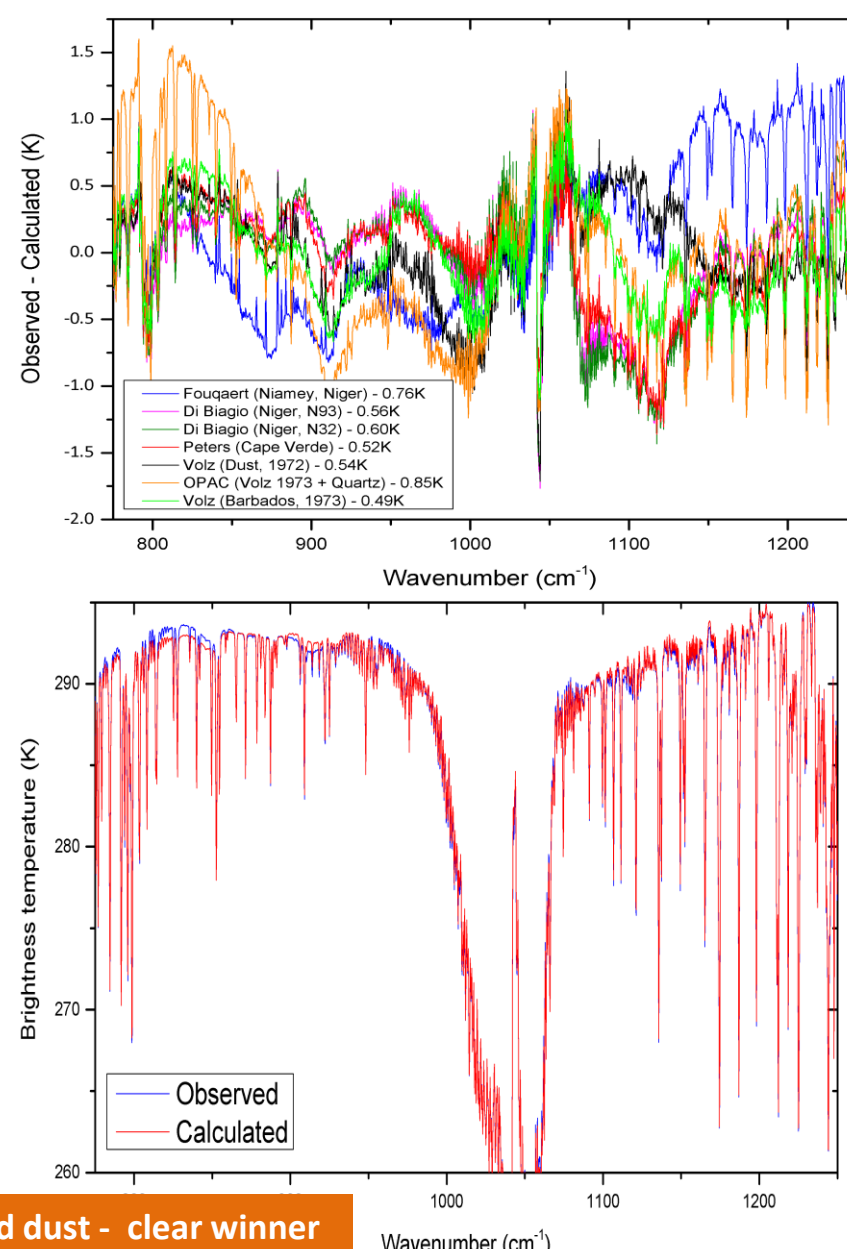
- Accurate** (in vs output)
- Comprehensive** (input)
- Representative** (input)

Reconstructing the spectrum

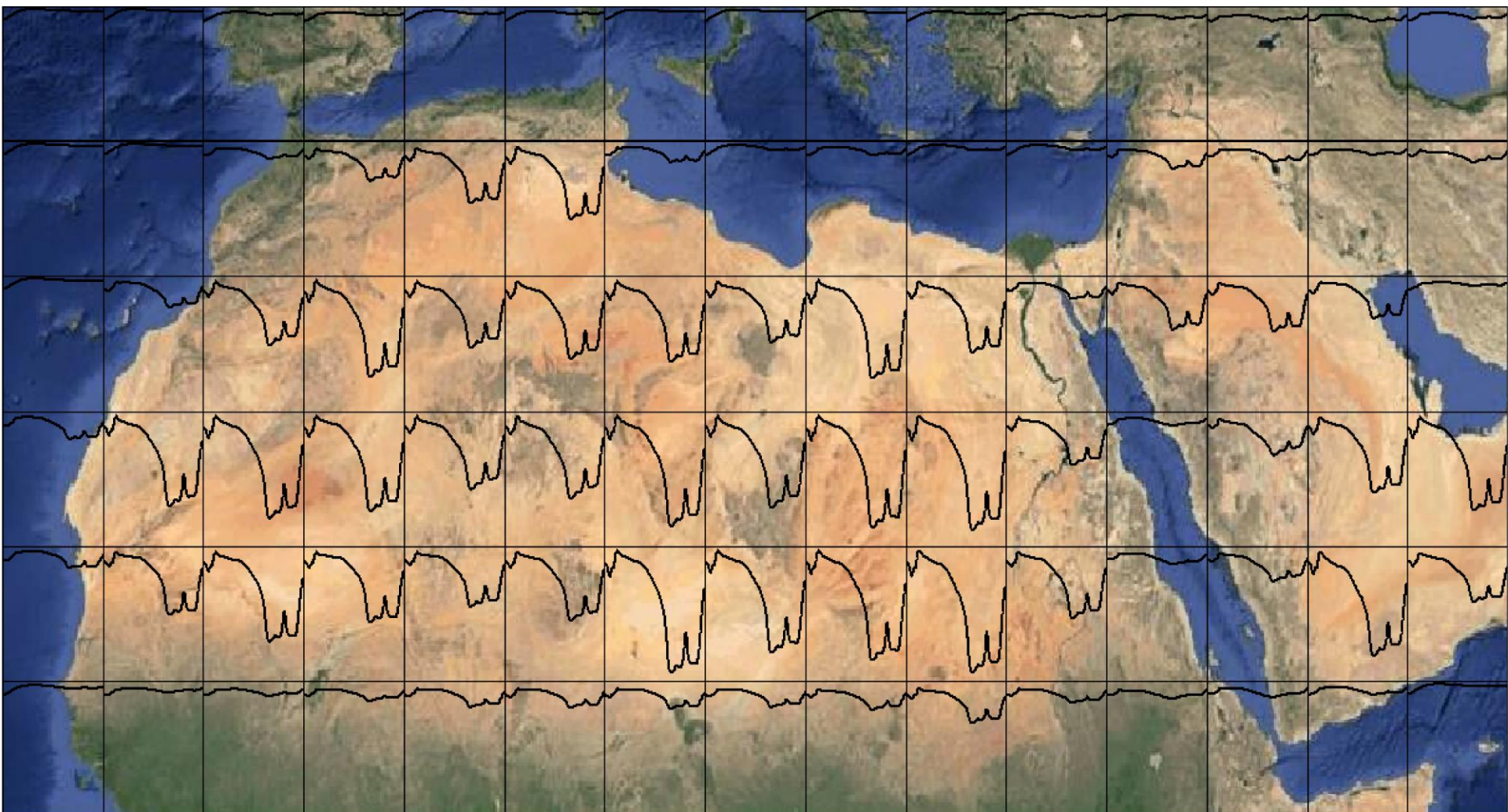


Example of imperfect forward model input

Description	Range cm ⁻¹	Reference
Measurements of aerosols		
Dust from precipitation (x, Germany and y, Bedford, Massachusetts)	250-50000	[Volz, 1972b] (figure), sample described in [Volz, 1972a], tabulated in [D'Almeida et al., 1991, Shettle & Fenn, 1979, World Meteorological Organization, 1986]. Termed 'insoluble' in [Hess et al., 1998, Koepke et al., 1997].
Dust (Meppen, Germany and Bedford, Massachusetts)	250-50000	[Volz, 1983] (figure)
Saharan dust Niamey, Niger	250-4000	[Fouquart et al., 1987] (figure) [Fouquart et al., 1984] (figure on different scale)
Saharan sand Barbados, West Indies	250-4000	[Volz, 1973] (figure)
Saharan sand Cape Verde, dry and 50% relative humidity	470-7000	[Peters, 2009]
Afghanistan, Tadzhikistan sand	400-4000	[Sokolik et al., 1993] (figure only, figure also in [Sokolik et al., 1998])
Negev, Israel clean and dust storm	833-1333	[Fischer, 1976], figure also in [Sokolik et al., 1998]
Dust in Southwester United States, Texas	625-10000	[Patterson, 1981], imaginary part only. Real part calculated and shown in [Sokolik et al., 1998].
Niger, Algeria, Tunisia and the Gobi desert	400-4000	[Di Biagio et al., 2014b, Di Biagio et al., 2014a]
Compilations & Mixtures		
Almeida mineral compilation, mainly Volz dust	250-4000	[D'Almeida et al., 1991], based on [Volz, 1972b, Grams et al., 1974]
GADS/OPAC mineral compilation, mainly Volz Sahara, with addition of extra Quartz absorption features	250-4000	[Koepke et al., 1997, Hess et al., 1998], based on [Levin & Lindberg, 1979, Volz, 1973, Patterson et al., 1977]
Averaged Arid Dust	250-50000	[Krekov, 1993] based on [Volz, 1983, Ivlev, 1982]
Mixture of hematite and quartz. Hematite is 10% by volume. O and E ray.	33-50000	[Longtin, 1988]
Composite clay (1/3 by weight of Montmorillonite, Illite and Kaolinite)	50-4000	[Querry, 1987]
Composite of Hematite, Illite, Montmorillonite, Quartz, Kaolinite and Calcite	100-34722	[Balkanski et al., 2007]



Example of imperfect forward model input

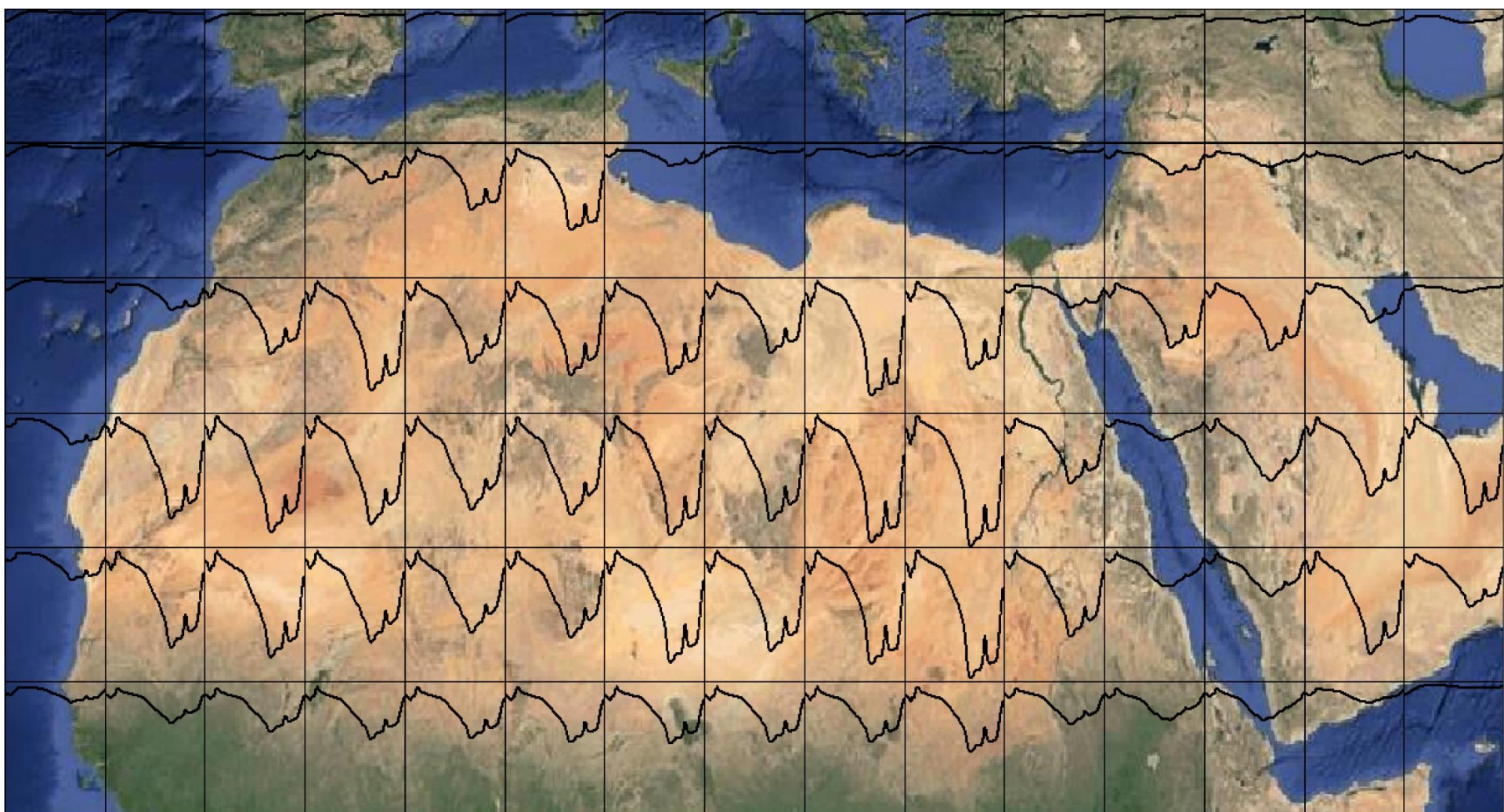


Emissivity in the 800 – 1200 cm range

November

Land: Zhou et al., 2011; Ocean: Nalli et al., 2008

Example of imperfect forward model input



June

Land: Zhou et al., 2011; Ocean: Nalli et al., 2008

Reconstructing the average dust signature

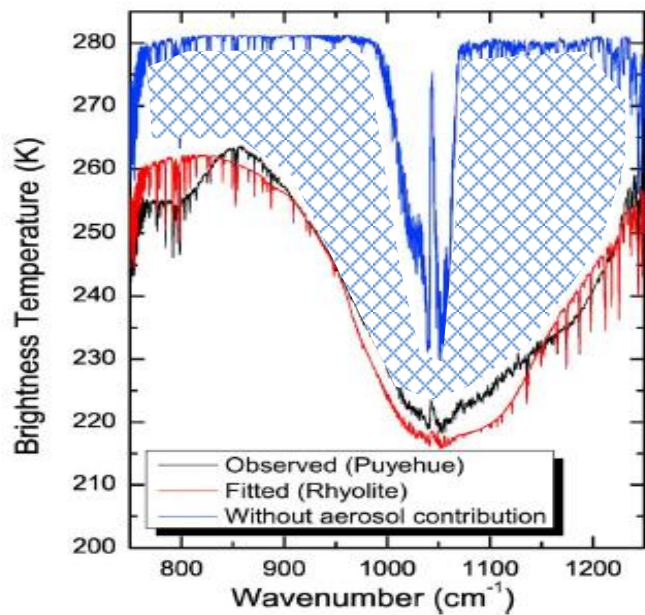
Brightness temperature difference

Singular value decomposition

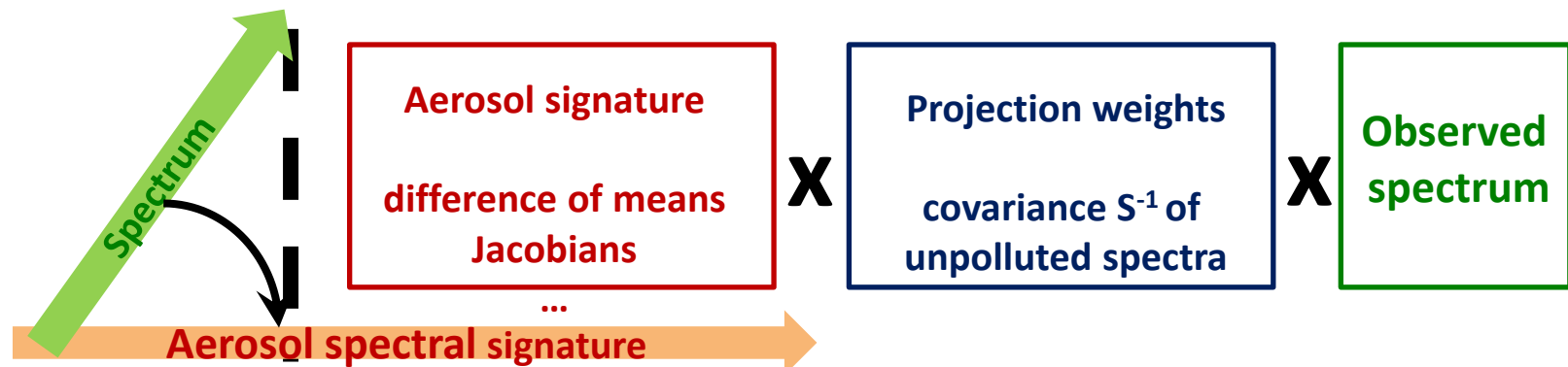
Principle component analysis

Linear discrimination analysis index

= minimizing forward model errors



Definition of dust index



This weighted projection unifies:

1. Linear discrimination analysis (LDA): $R = (\mu_k - \mu_l)^T S^{-1}(y)$
2. Weighted least squares: $(k)^T S^{-1}(y)$ (Walker et al, 2010)
3. PCA detection, uses different projection weights (Hurley et al., 2009)

$$R(y) = \frac{k^T S^{-1}(y - \mu_c)}{\sqrt{k^T S^{-1} k}}$$

- + No Forward model used
- + Emissivity Correction

INPUT
DATA

Auxiliary data

Dust height

Viewing angle

Temperature profile

Pressure profiles

Humidity profile

Emissivity

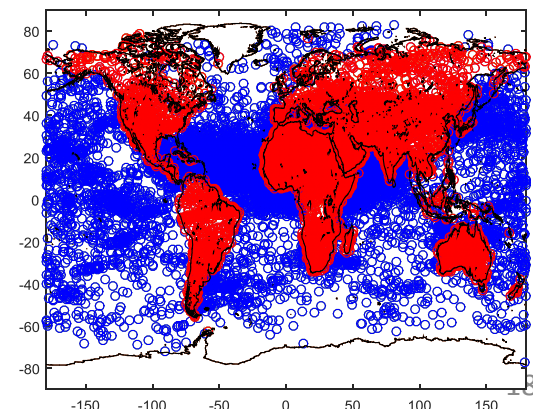
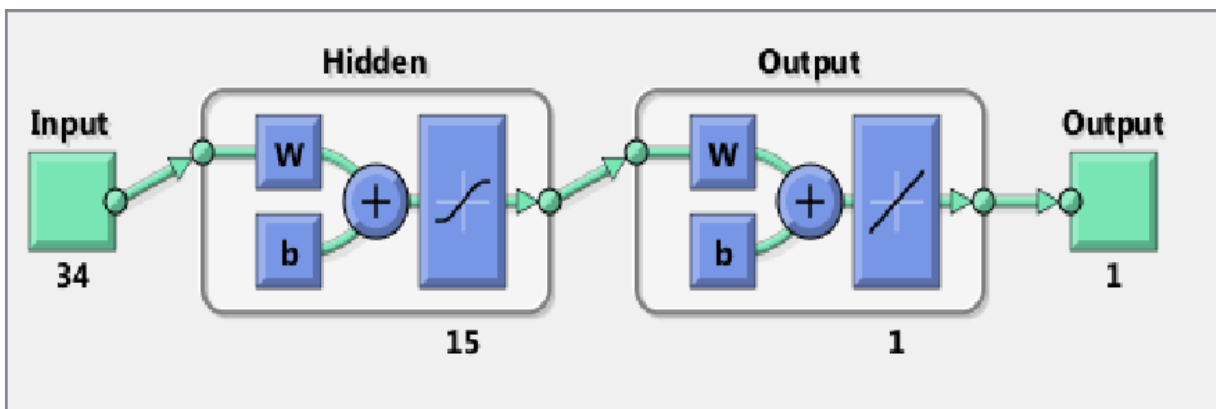
Radiance data

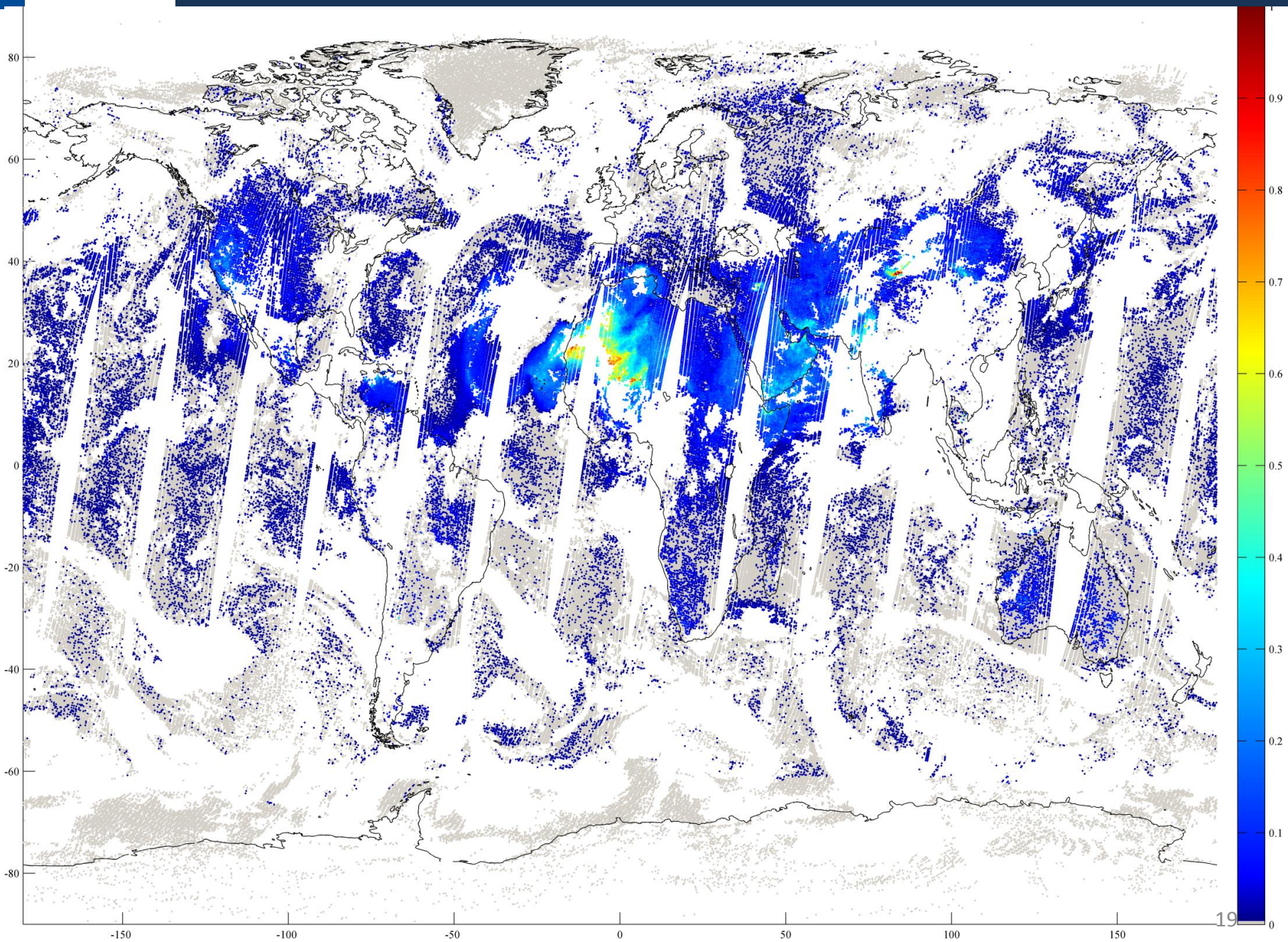
Dust index + couple of channels

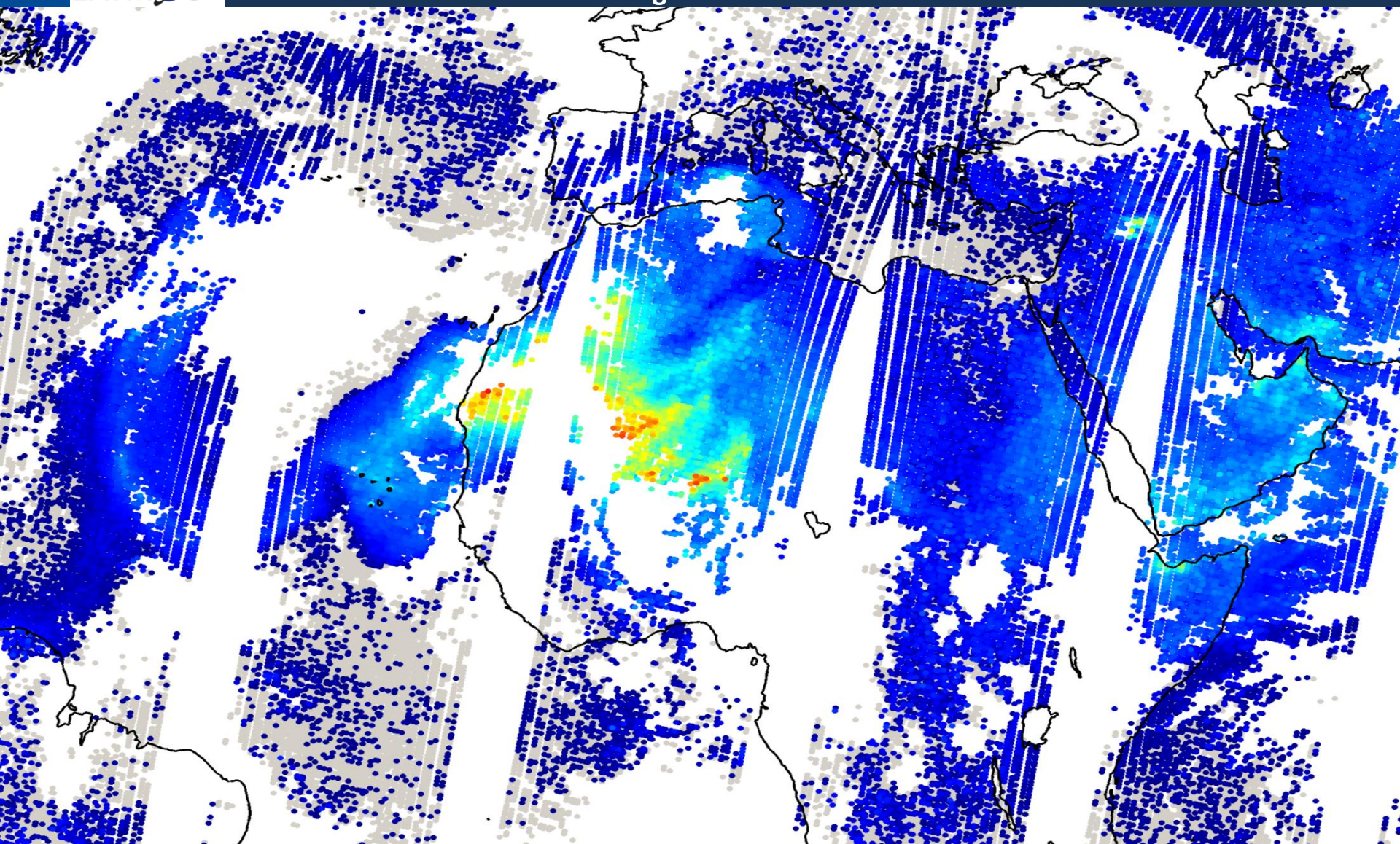
OUTPUT
DATA

Optical depth

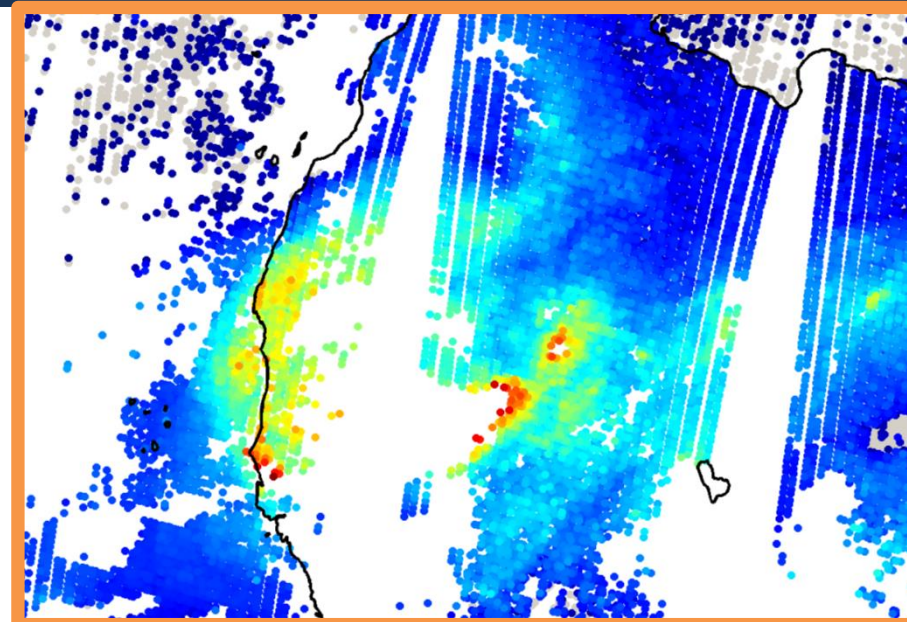
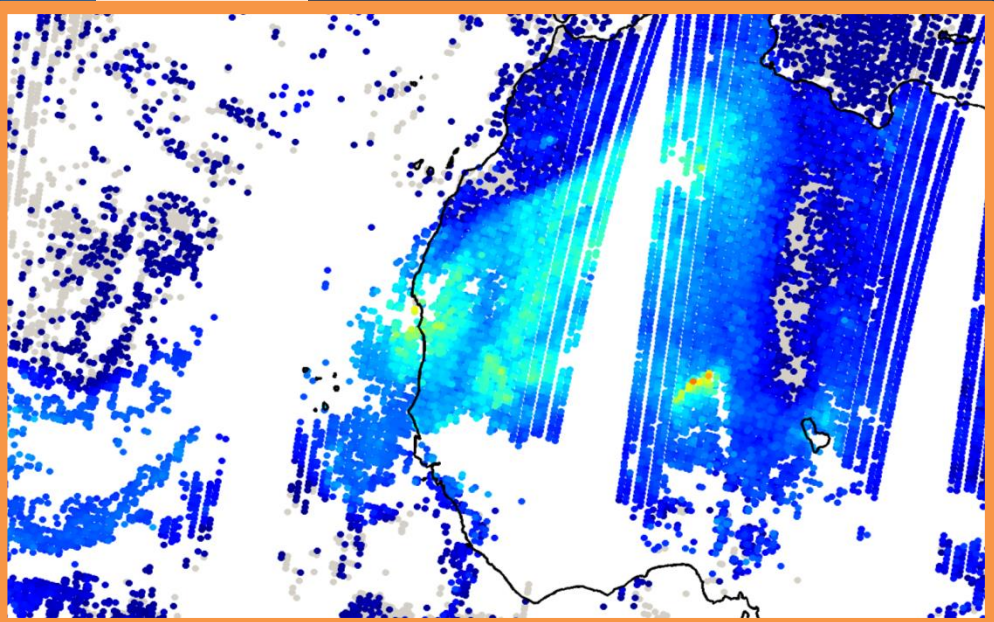
At 10 μm





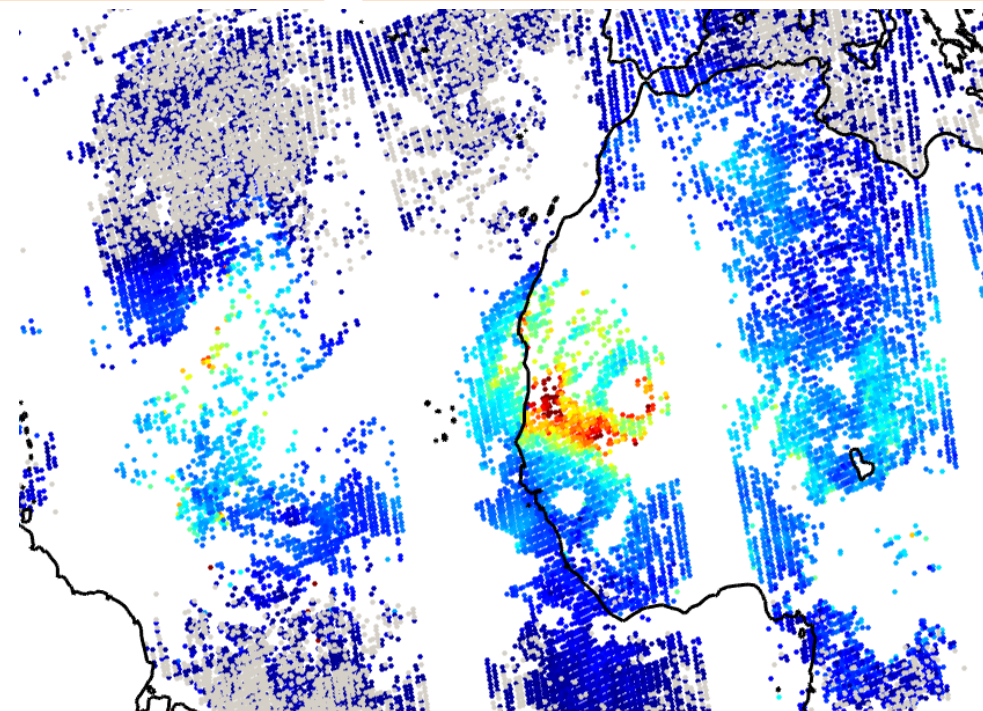


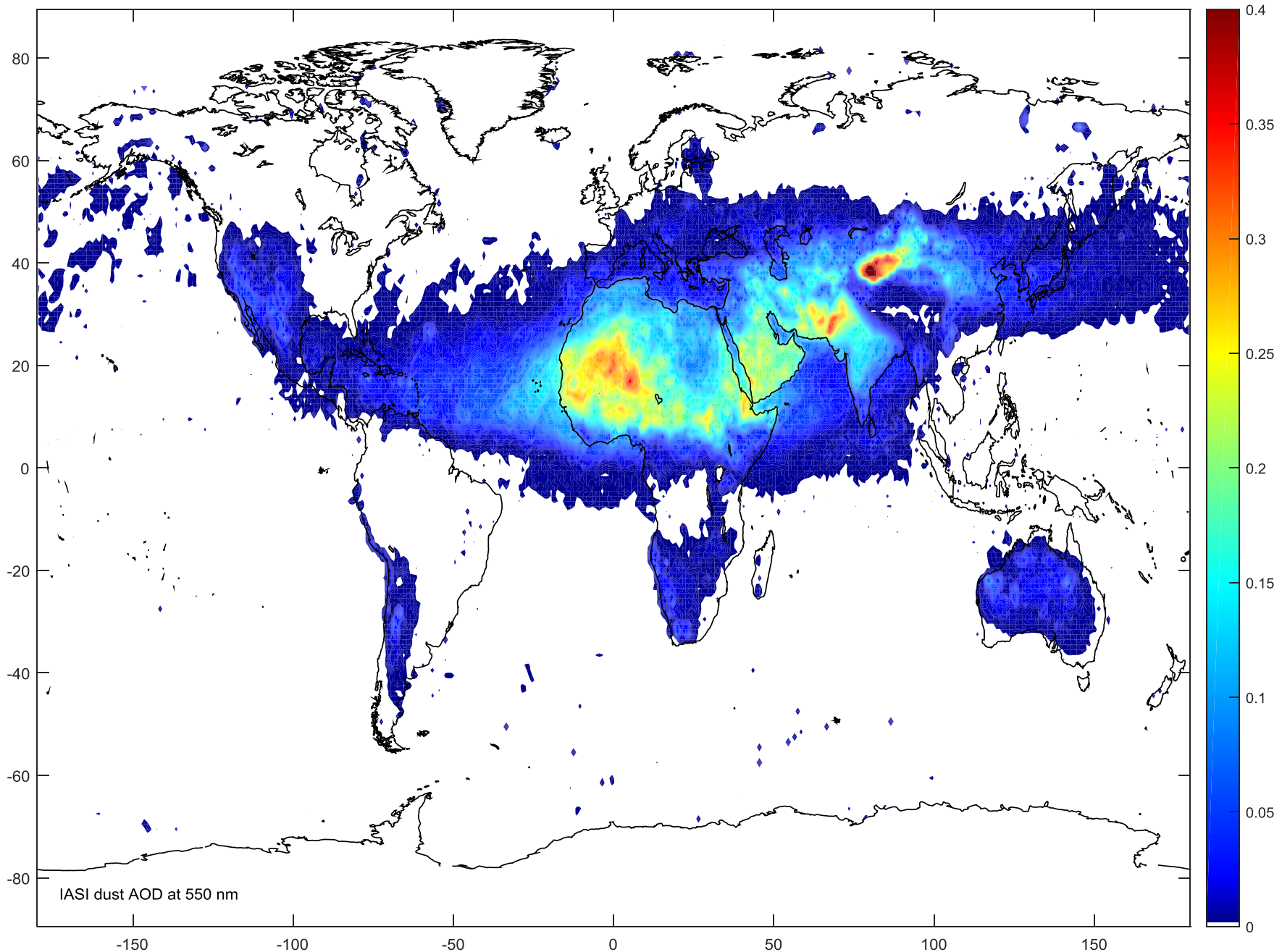
“Natural” plume edges

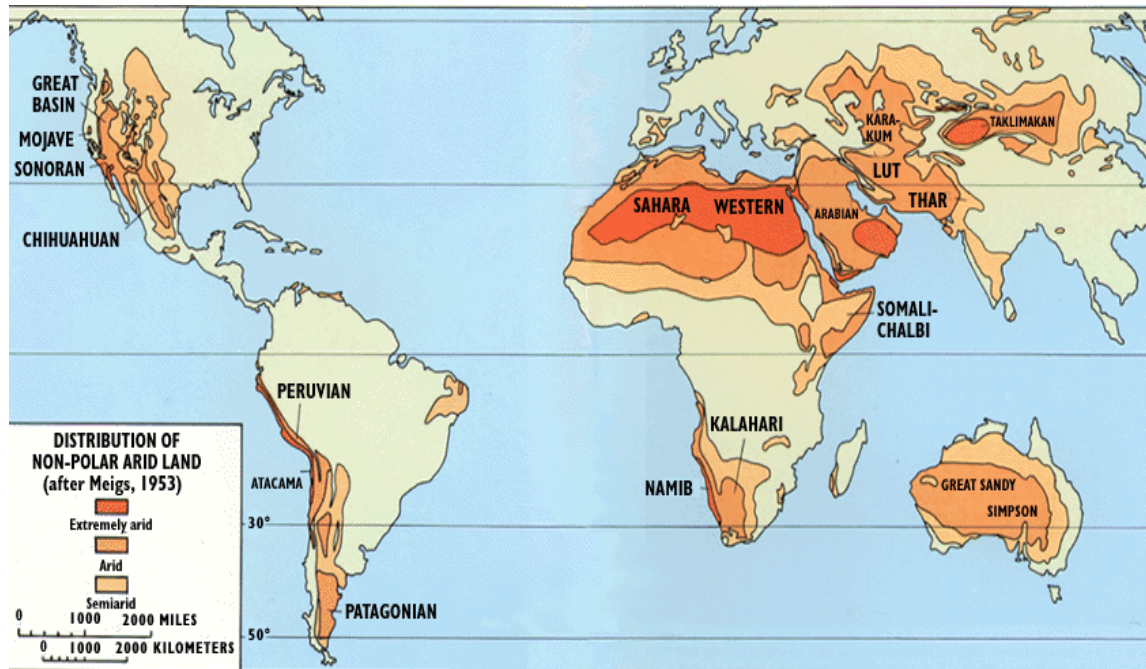
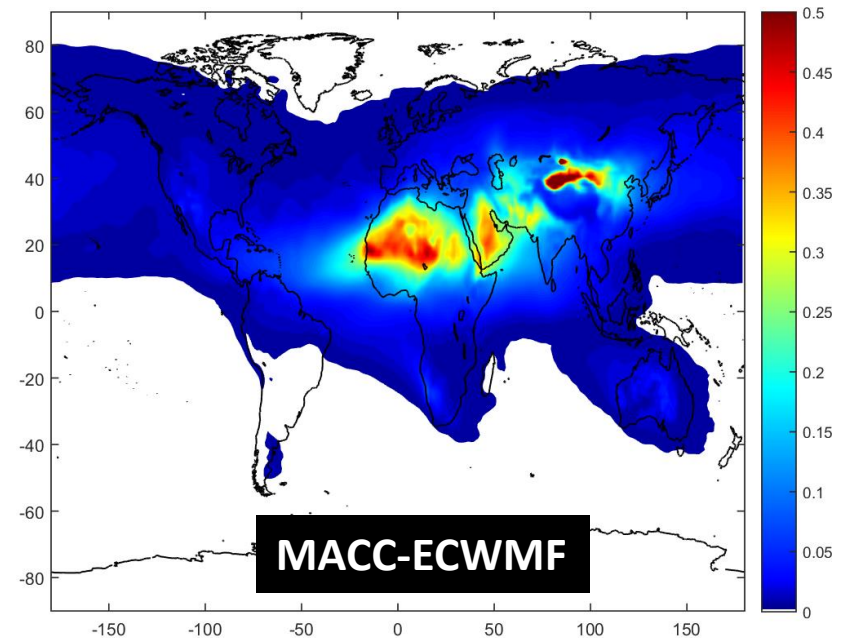
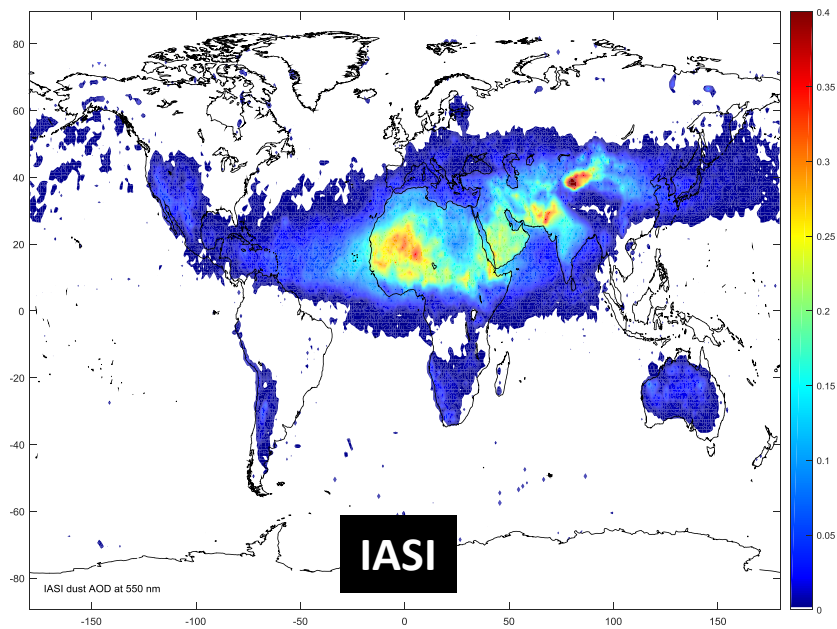


Good ocean/land continuity during daytime.

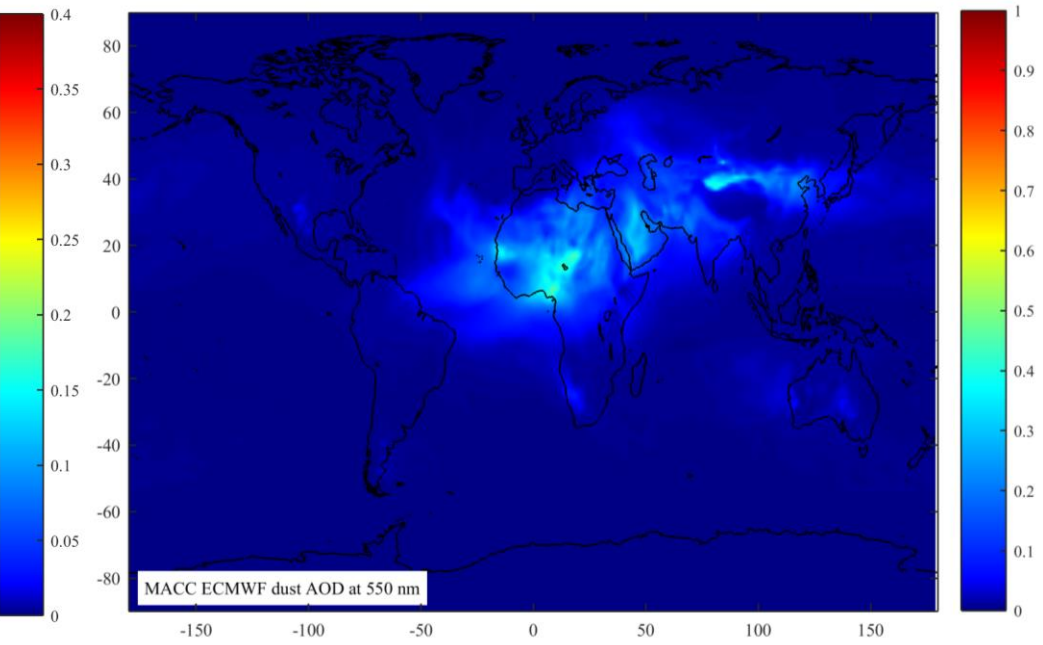
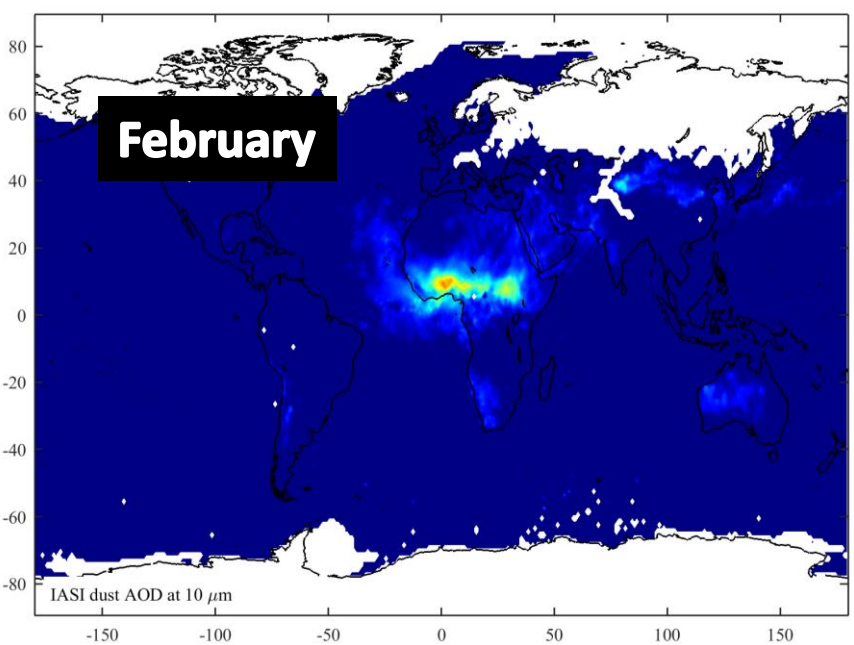
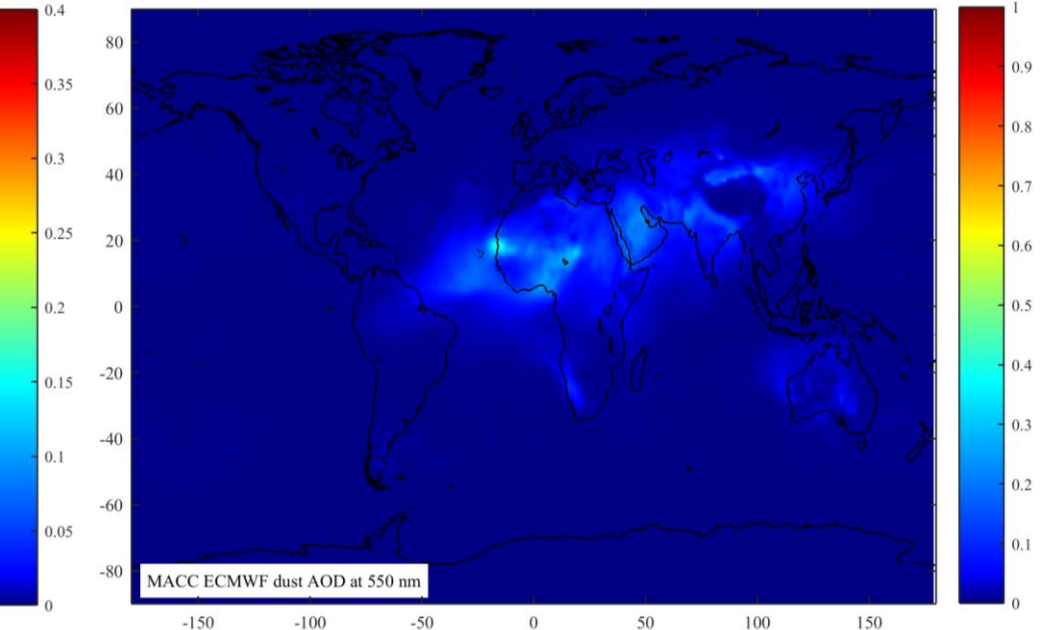
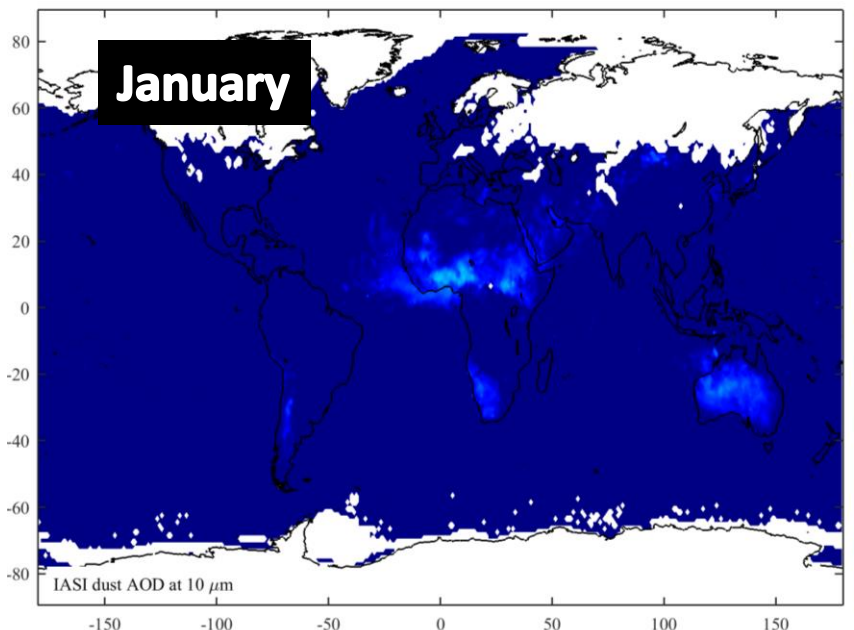
Not as good during nighttime!

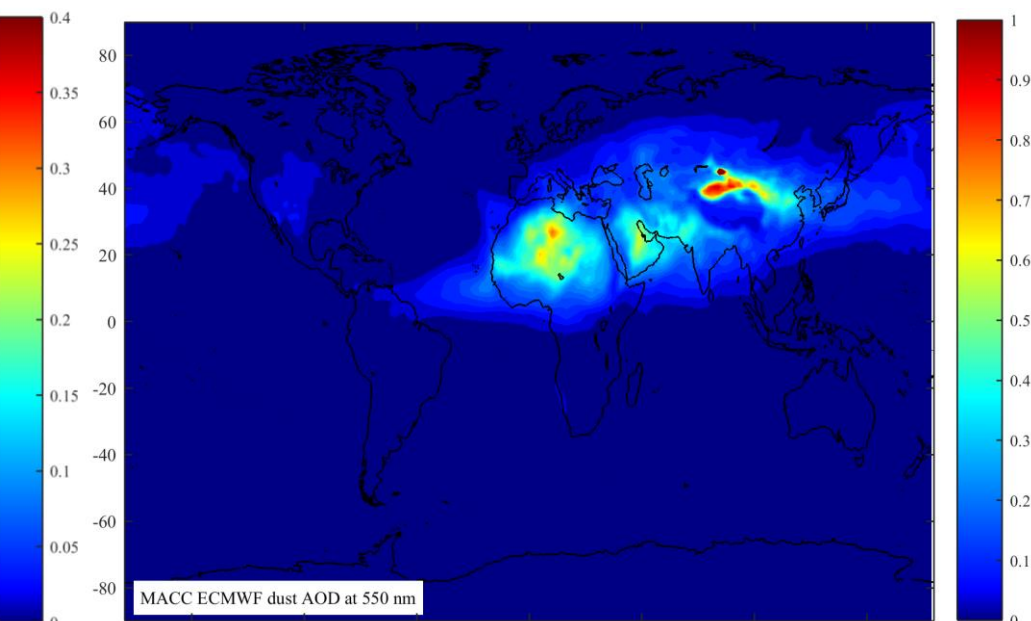
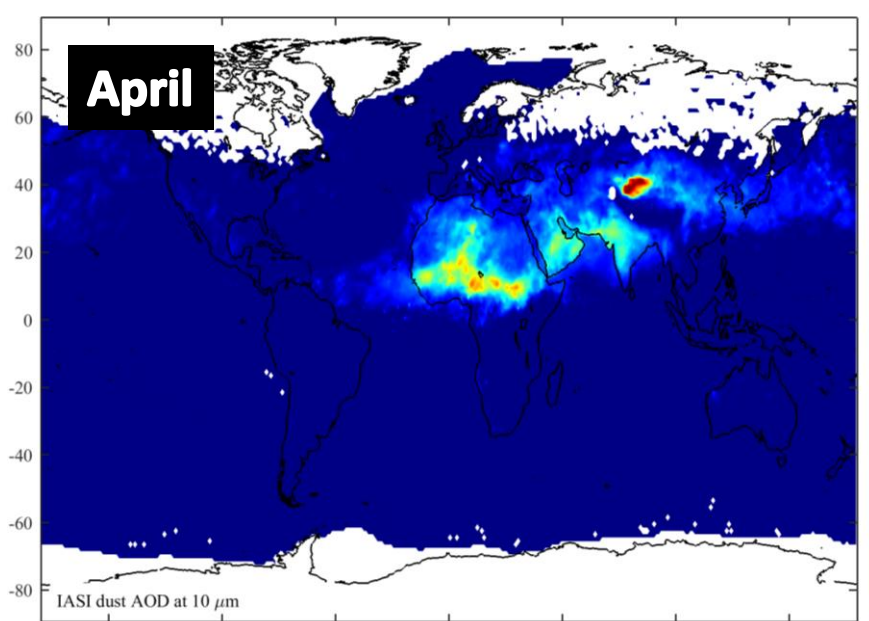
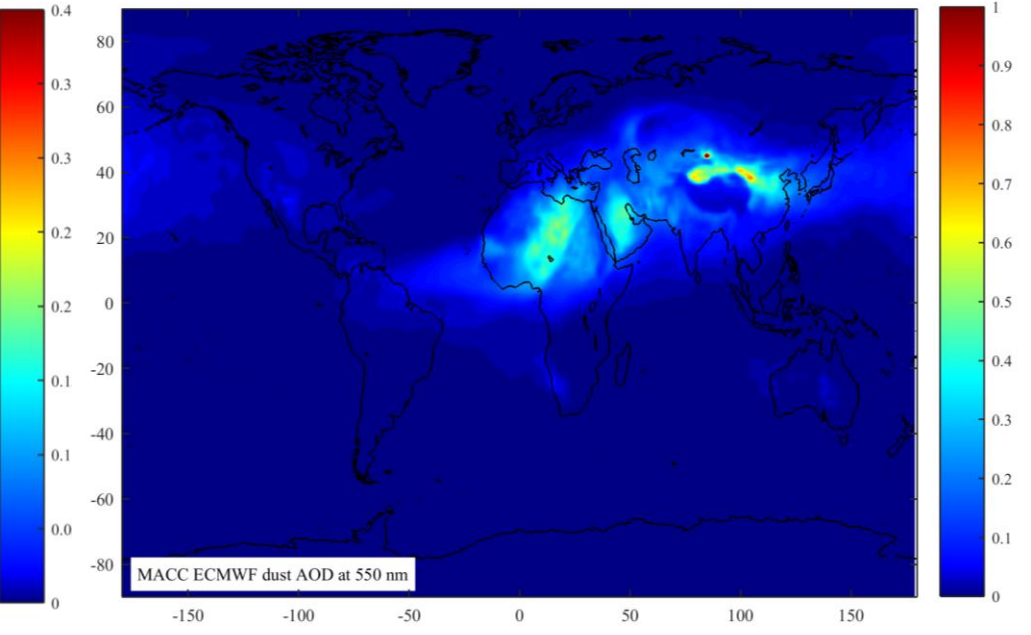
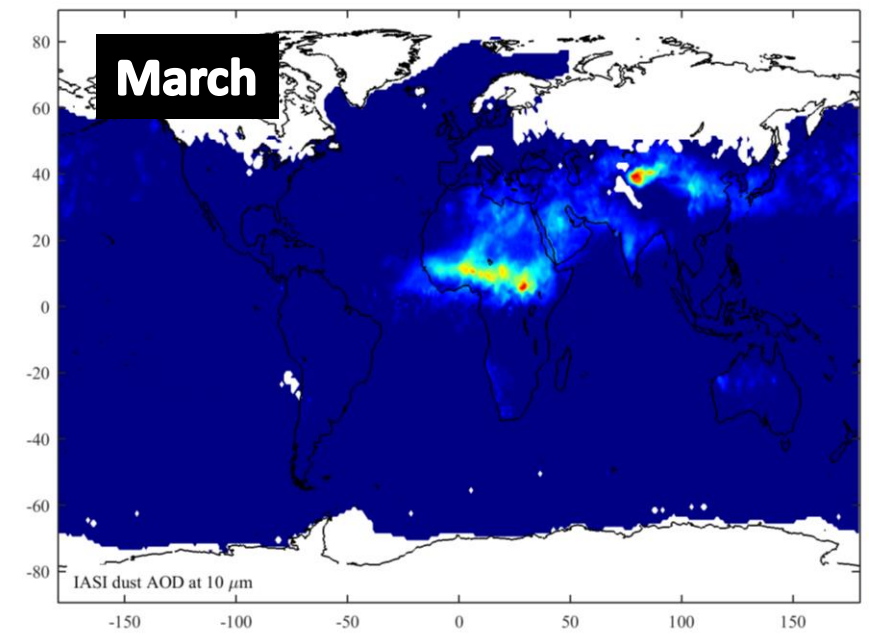


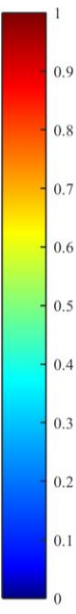
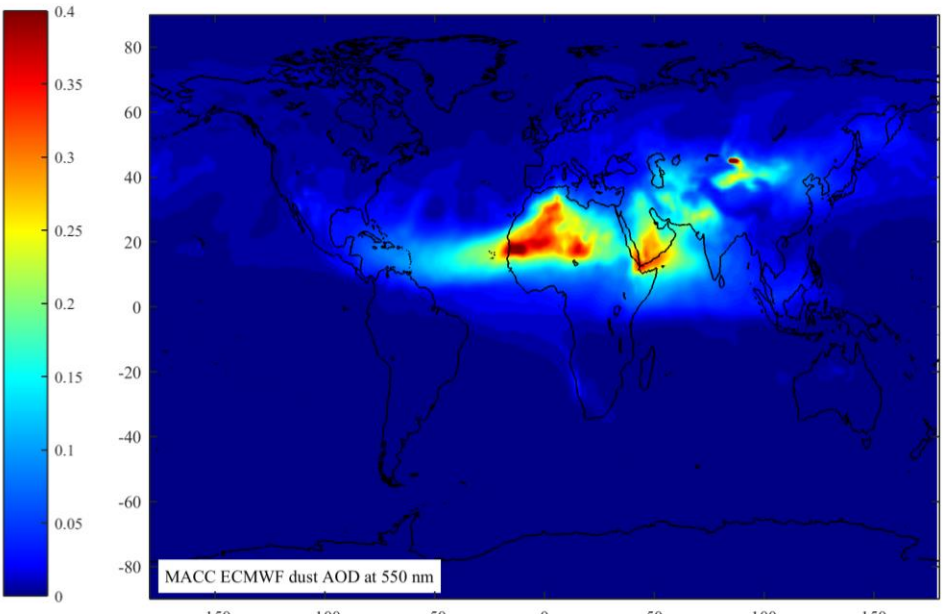
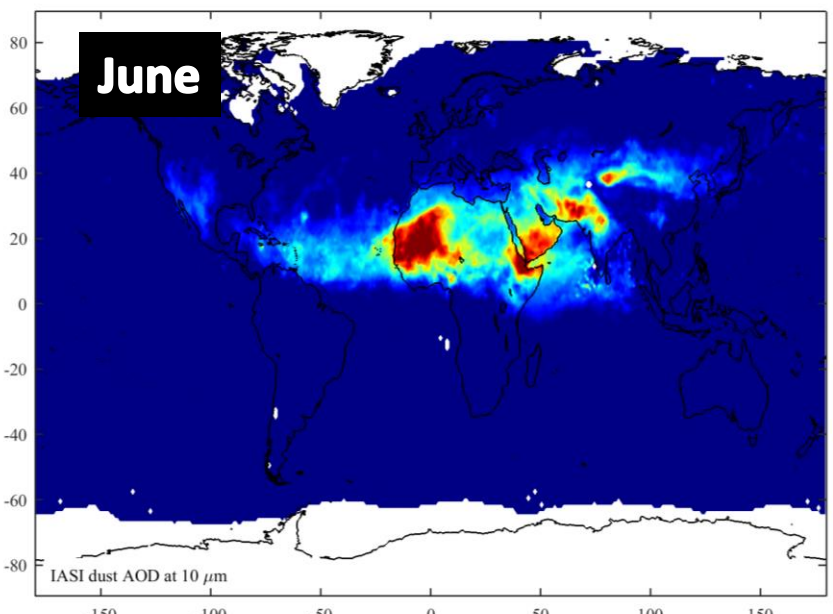
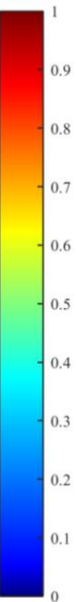
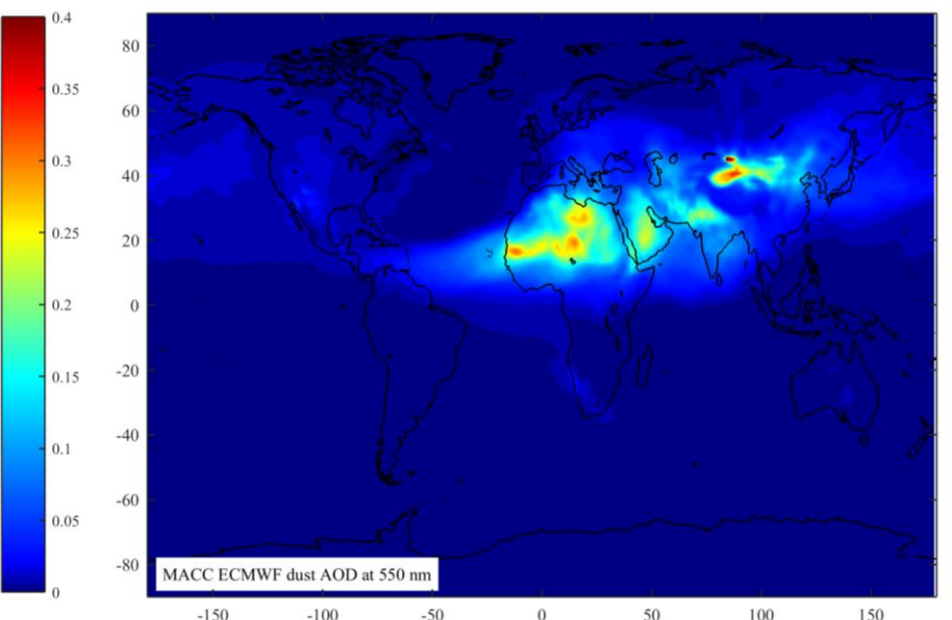
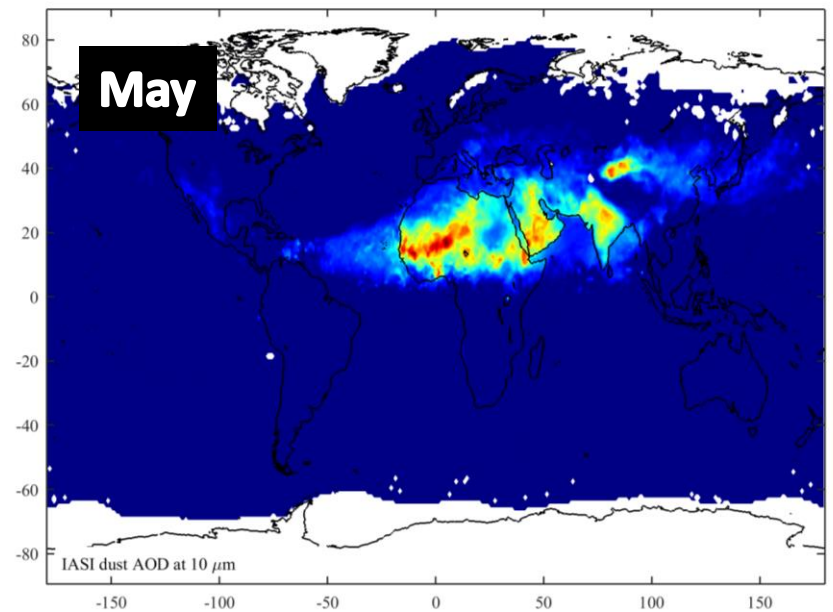


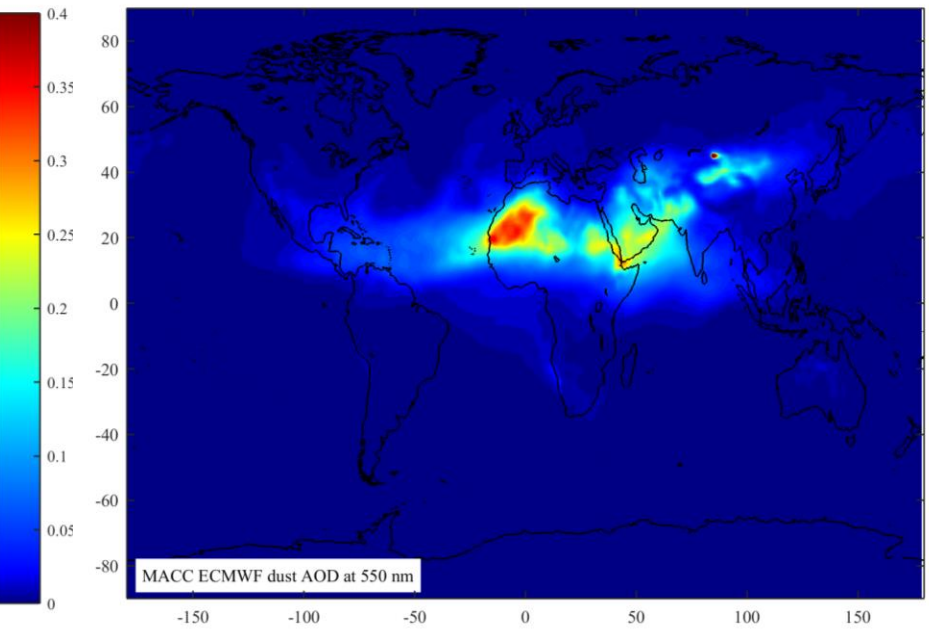
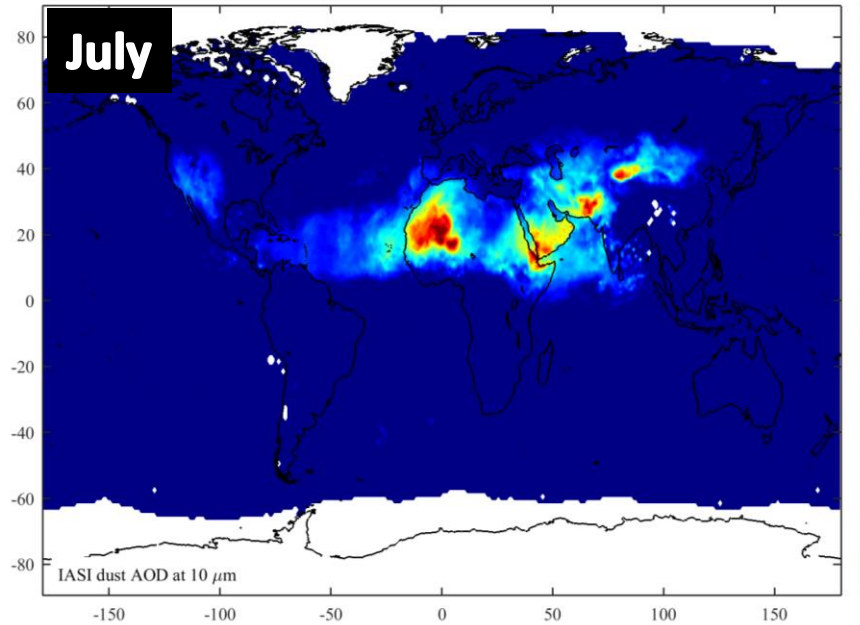
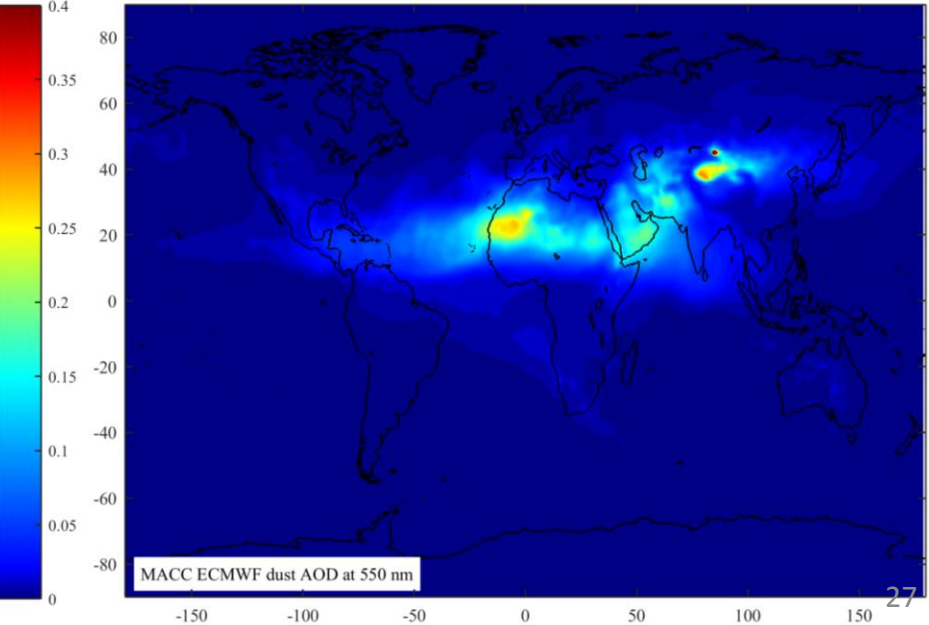
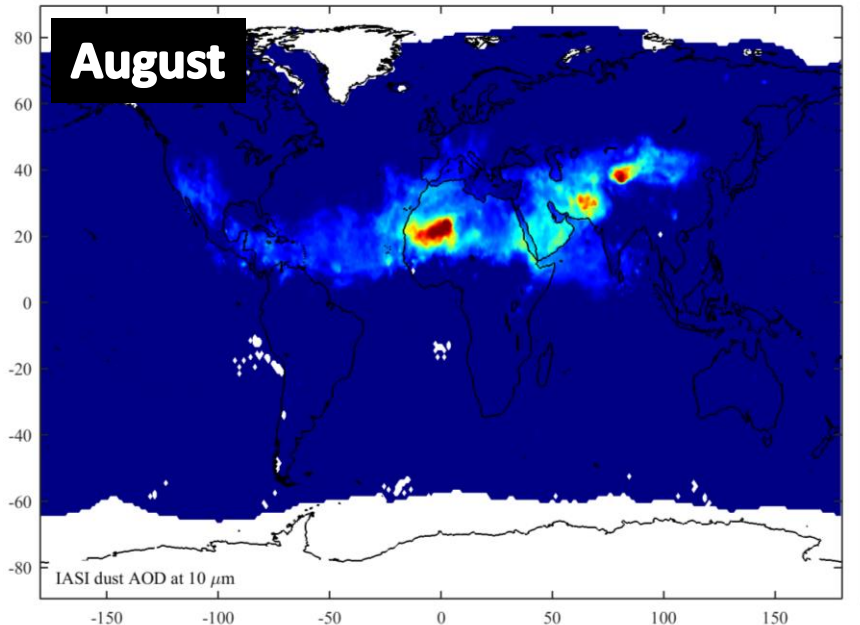


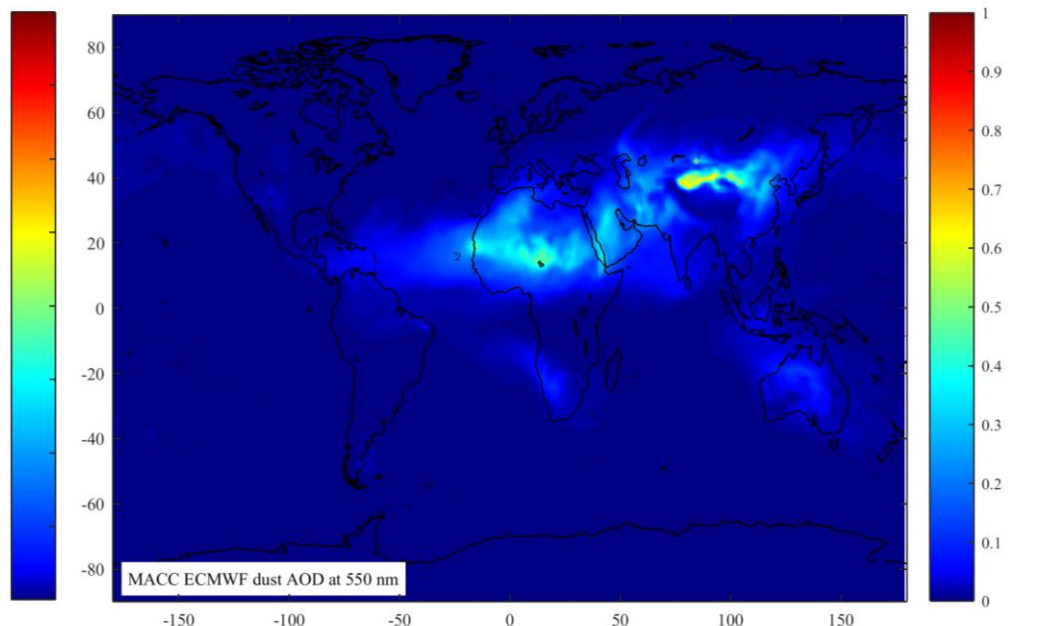
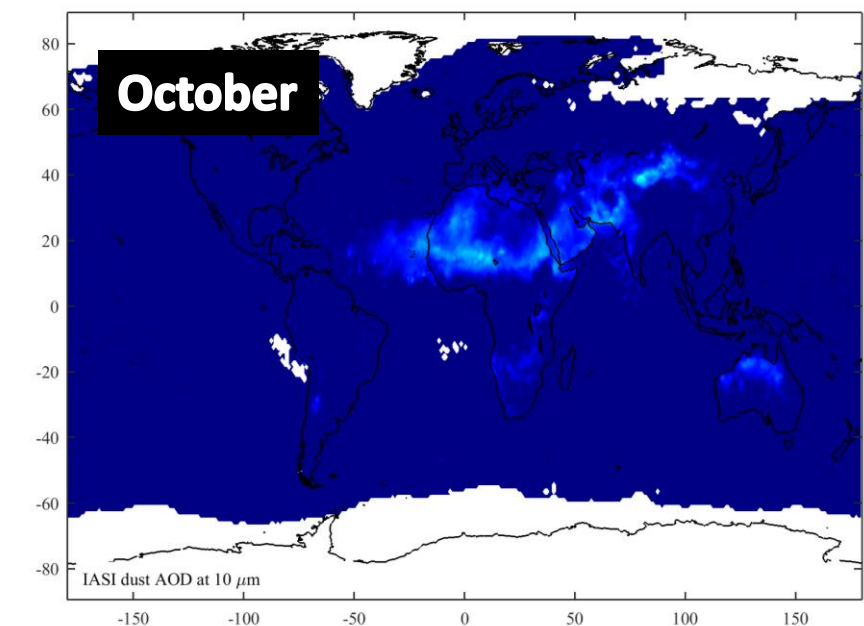
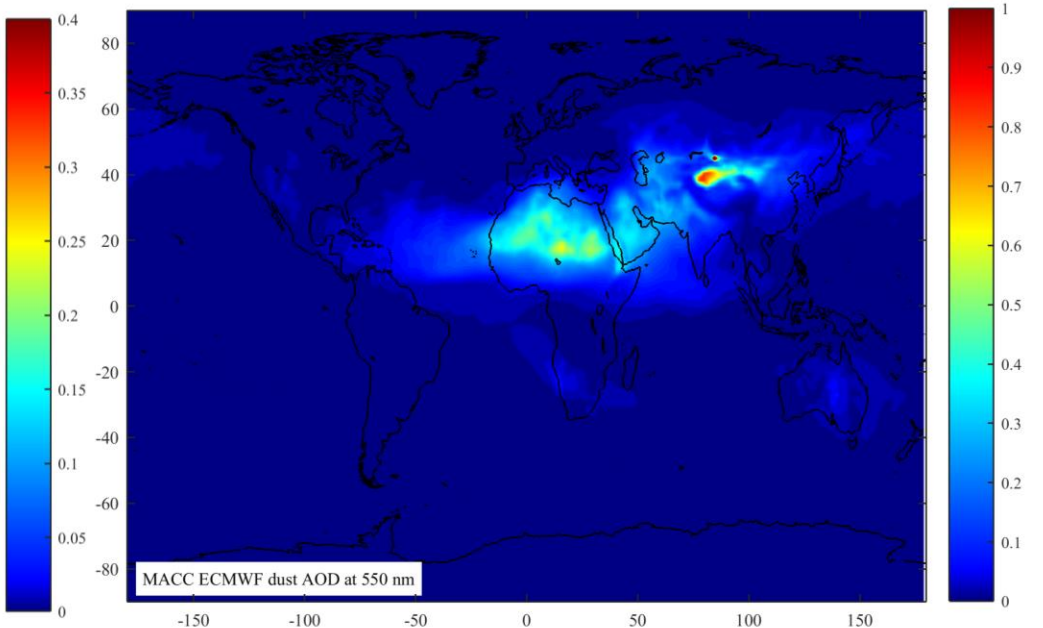
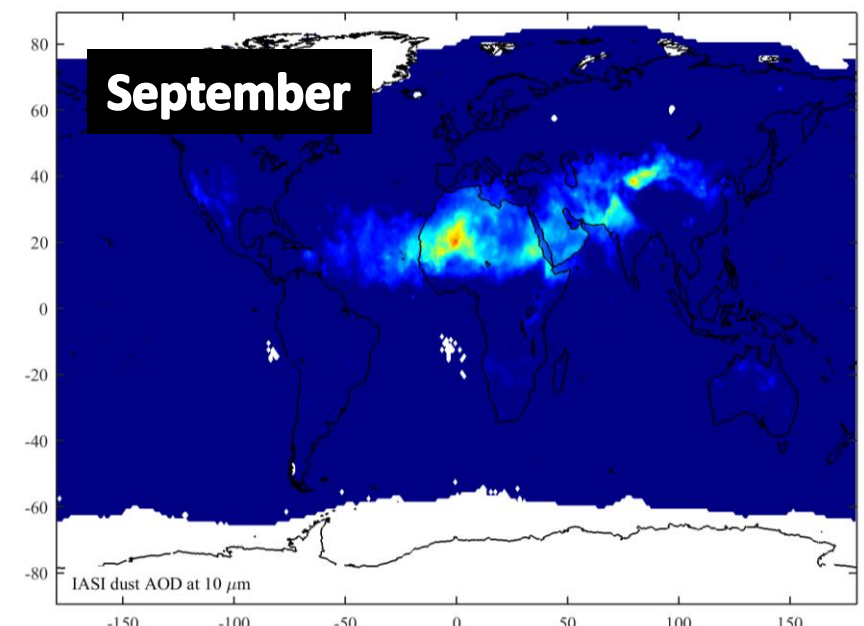
Note: Very robust
(dust where dust
should be and no dust
where no dust
expected)

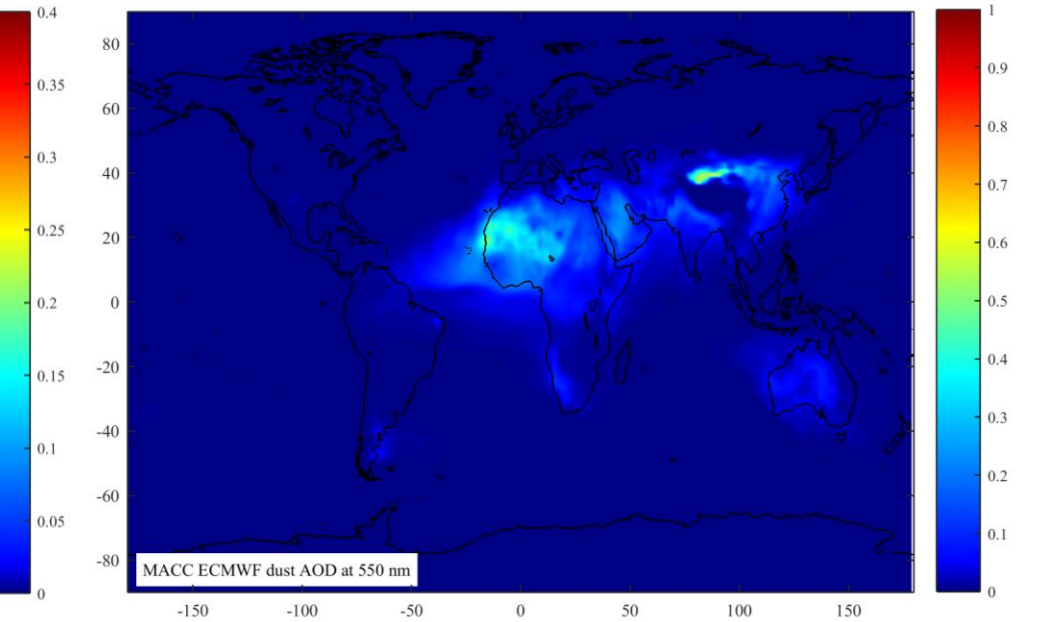
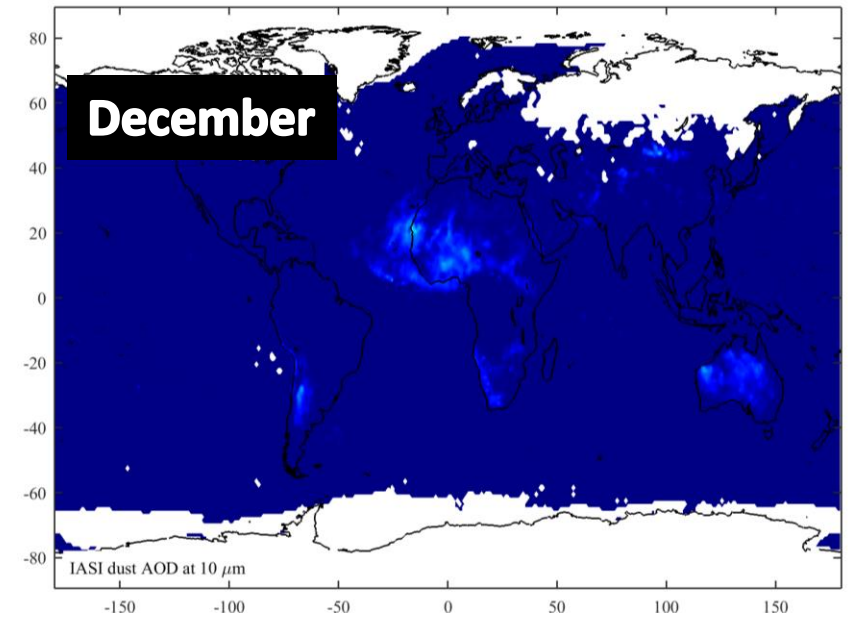
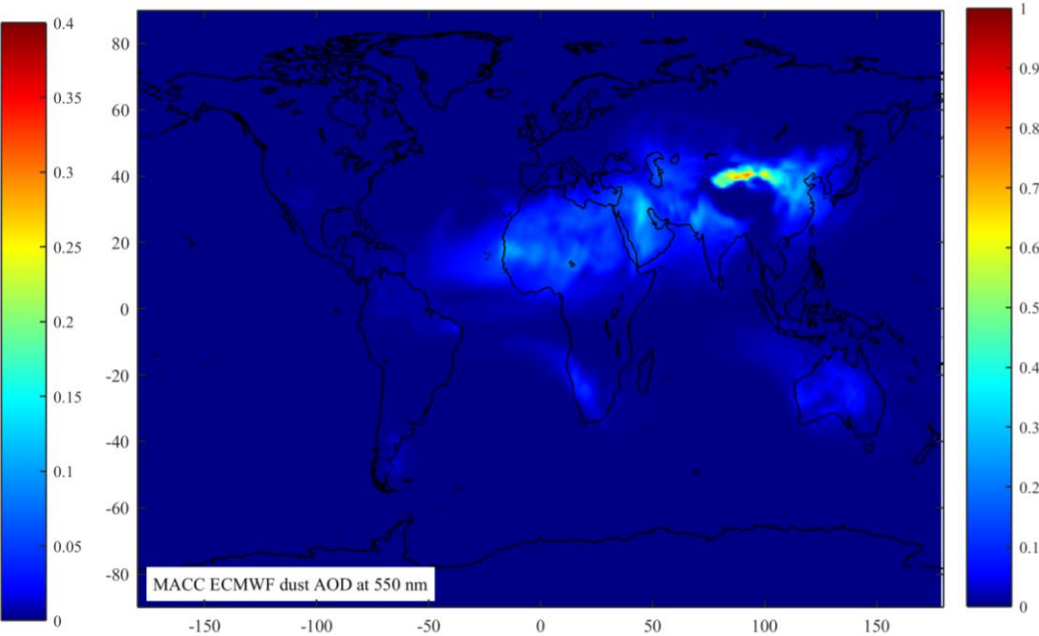
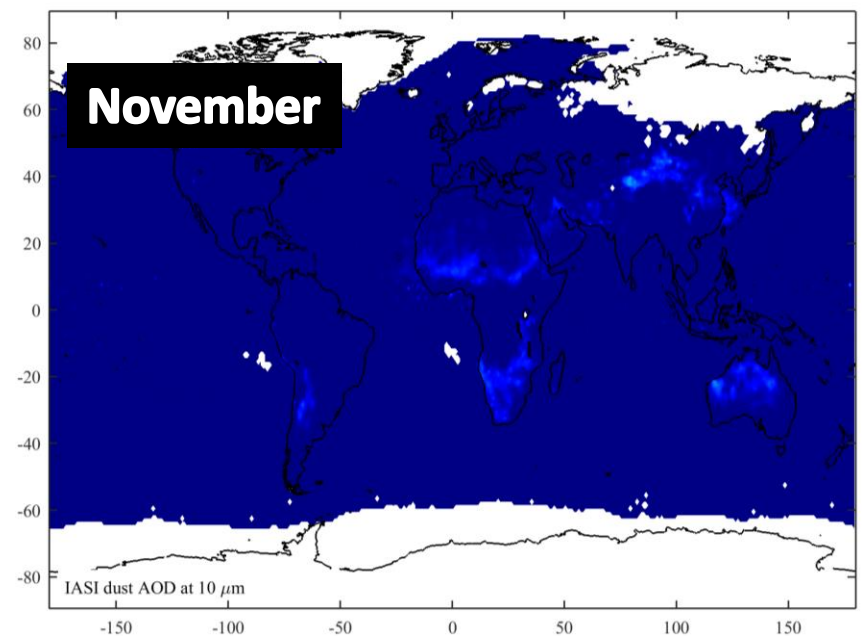


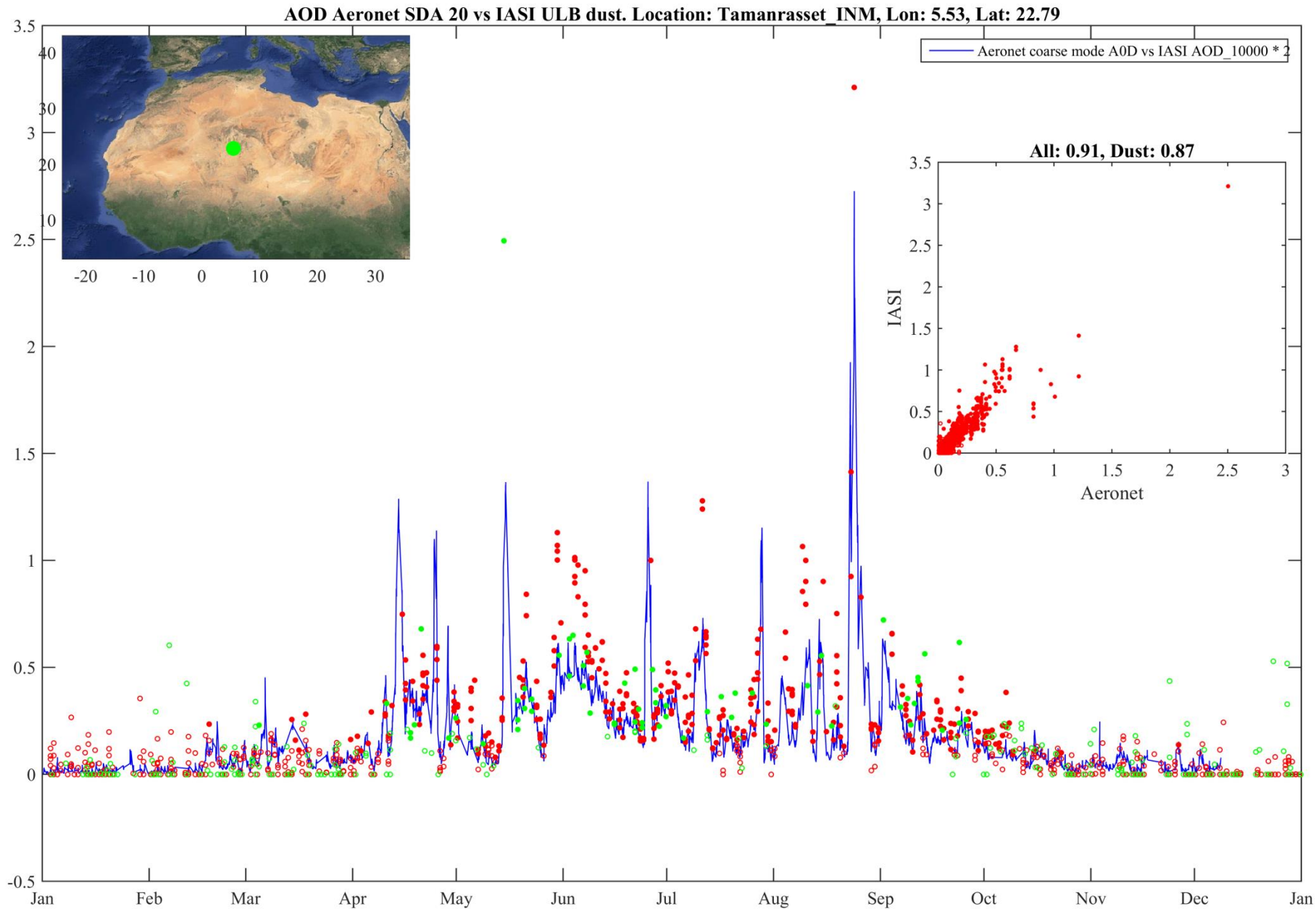


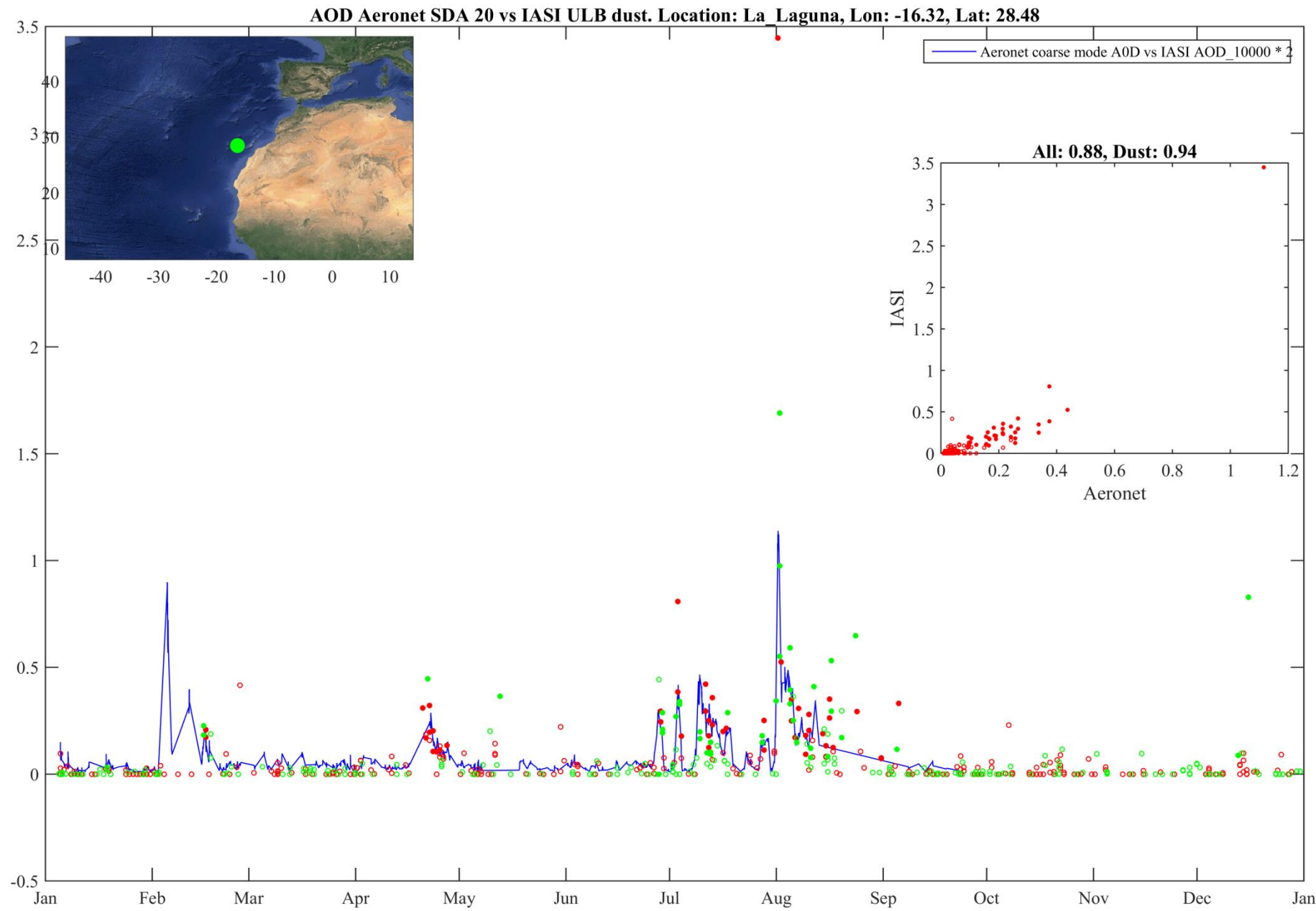


July**August**

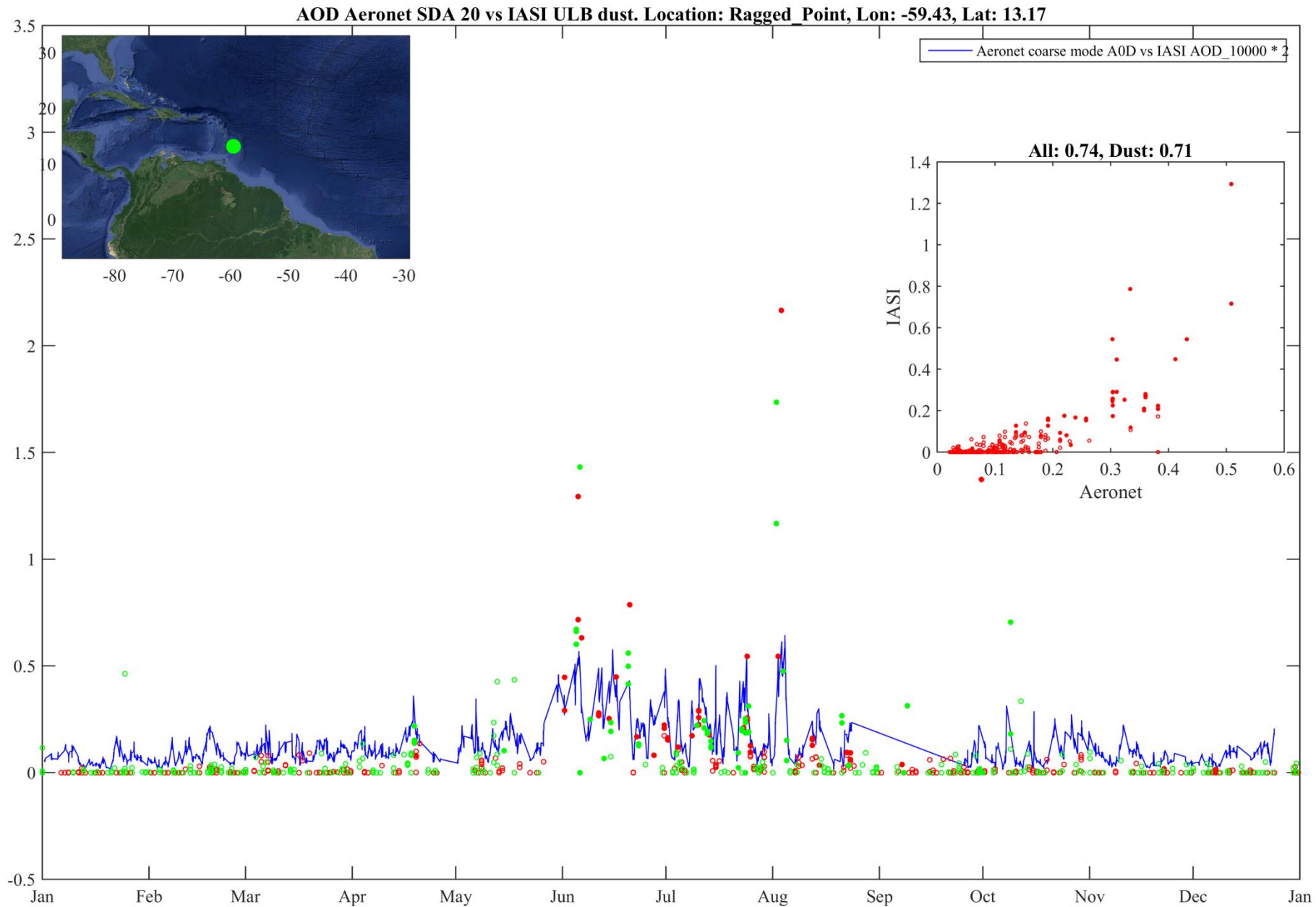


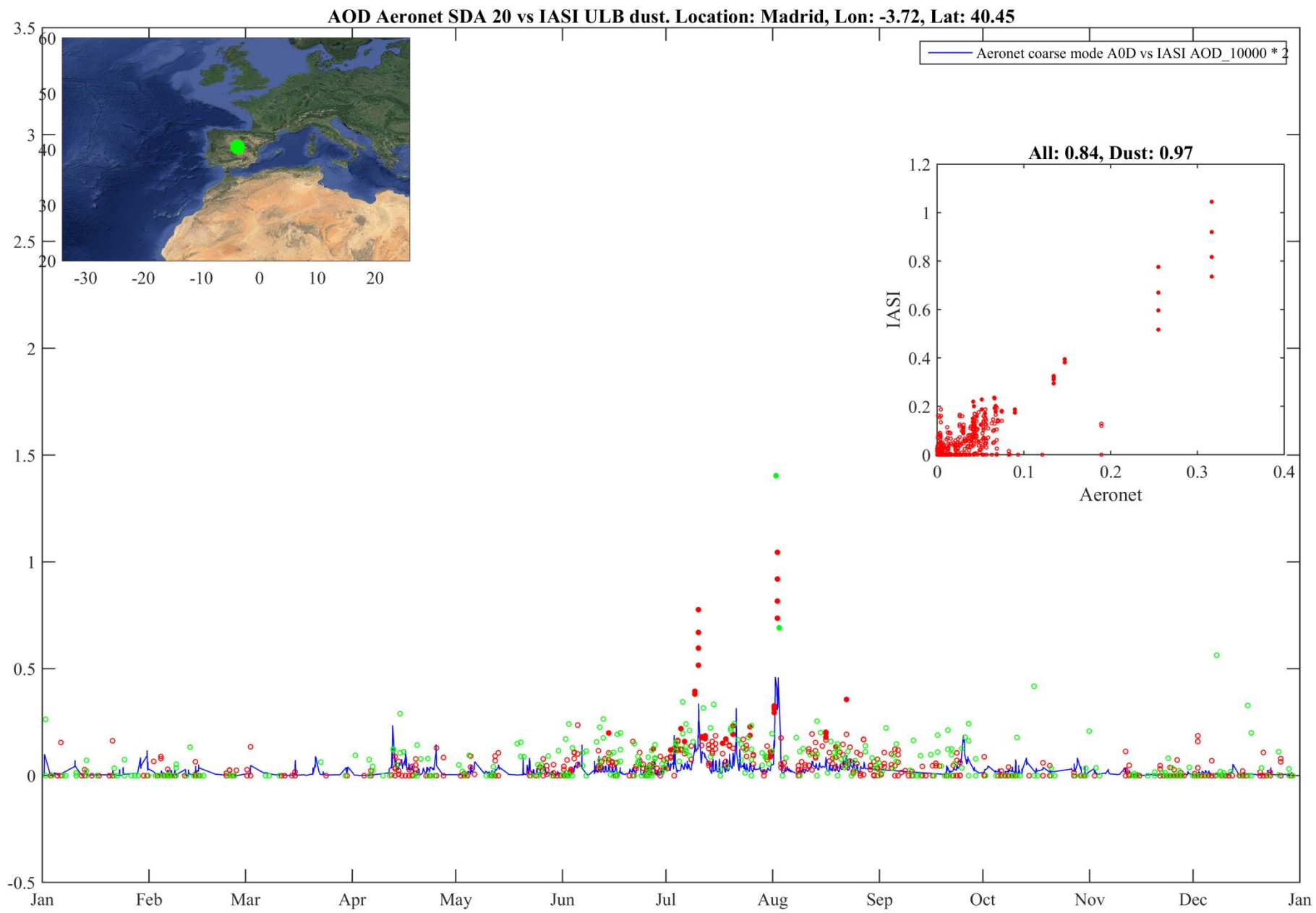


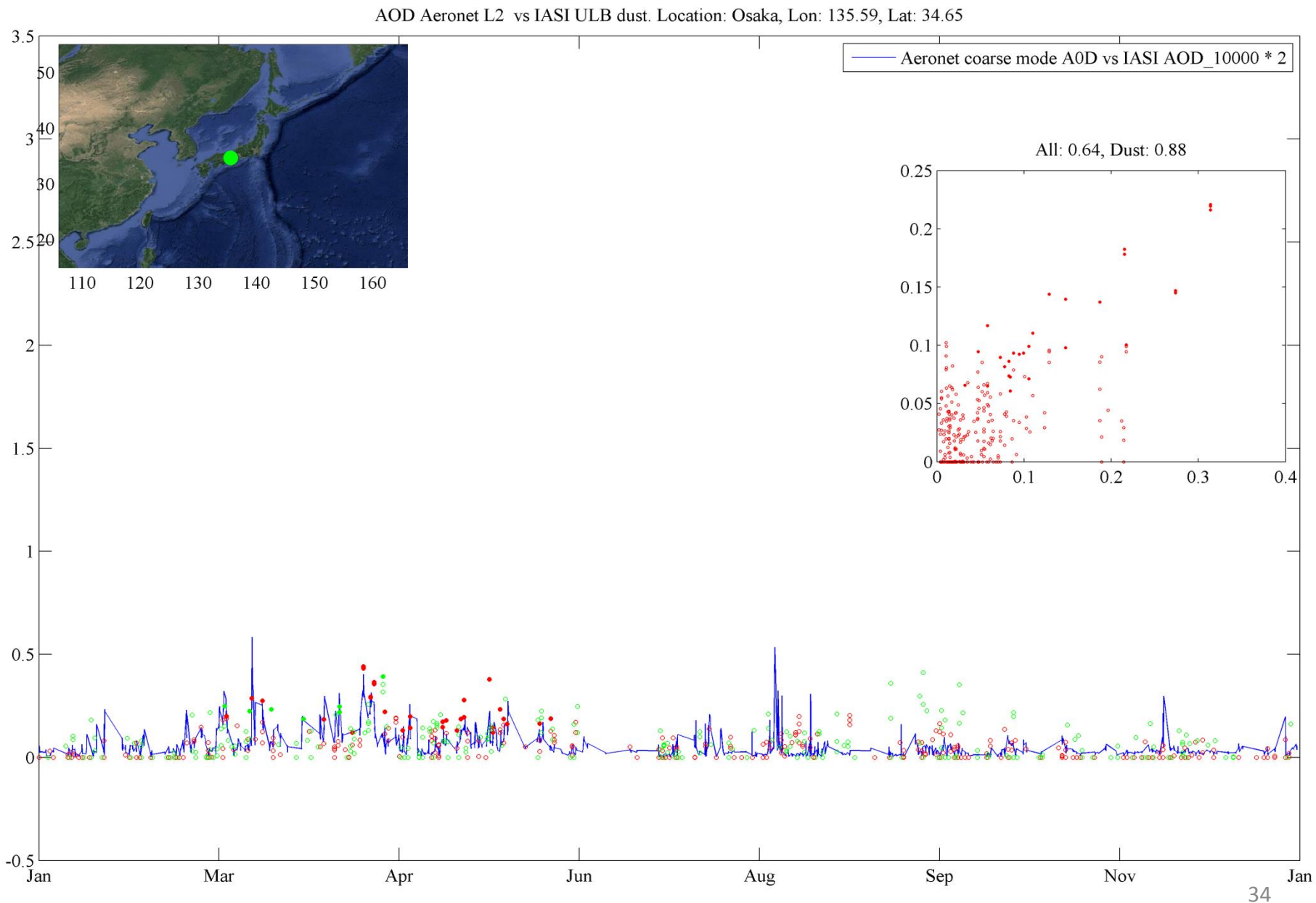


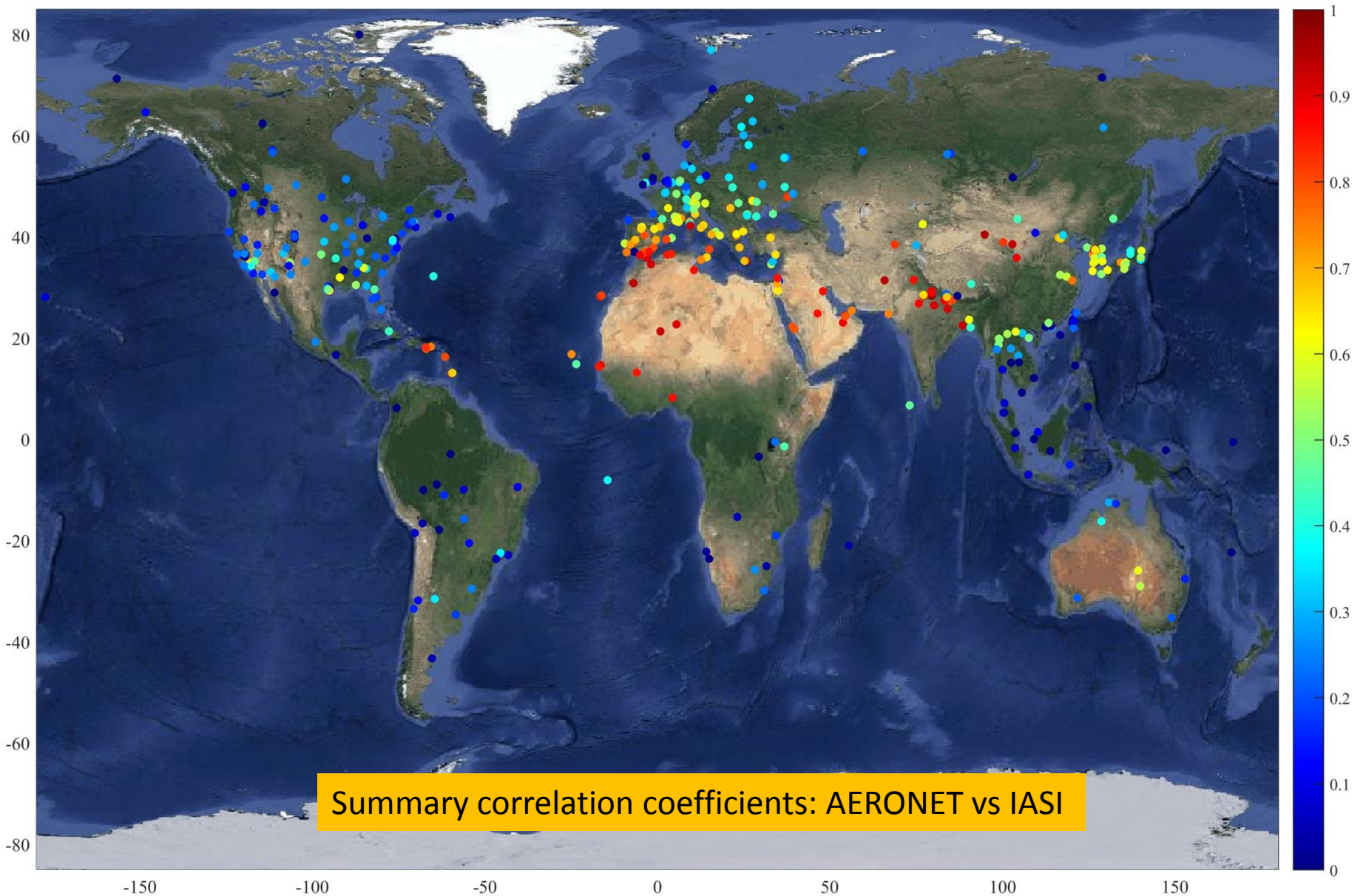


AOD Aeronet SDA 20 vs IASI ULB dust. Location: Ragged Point, Lon: -59.43, Lat: 13.17









Round up

Theoretical advantages

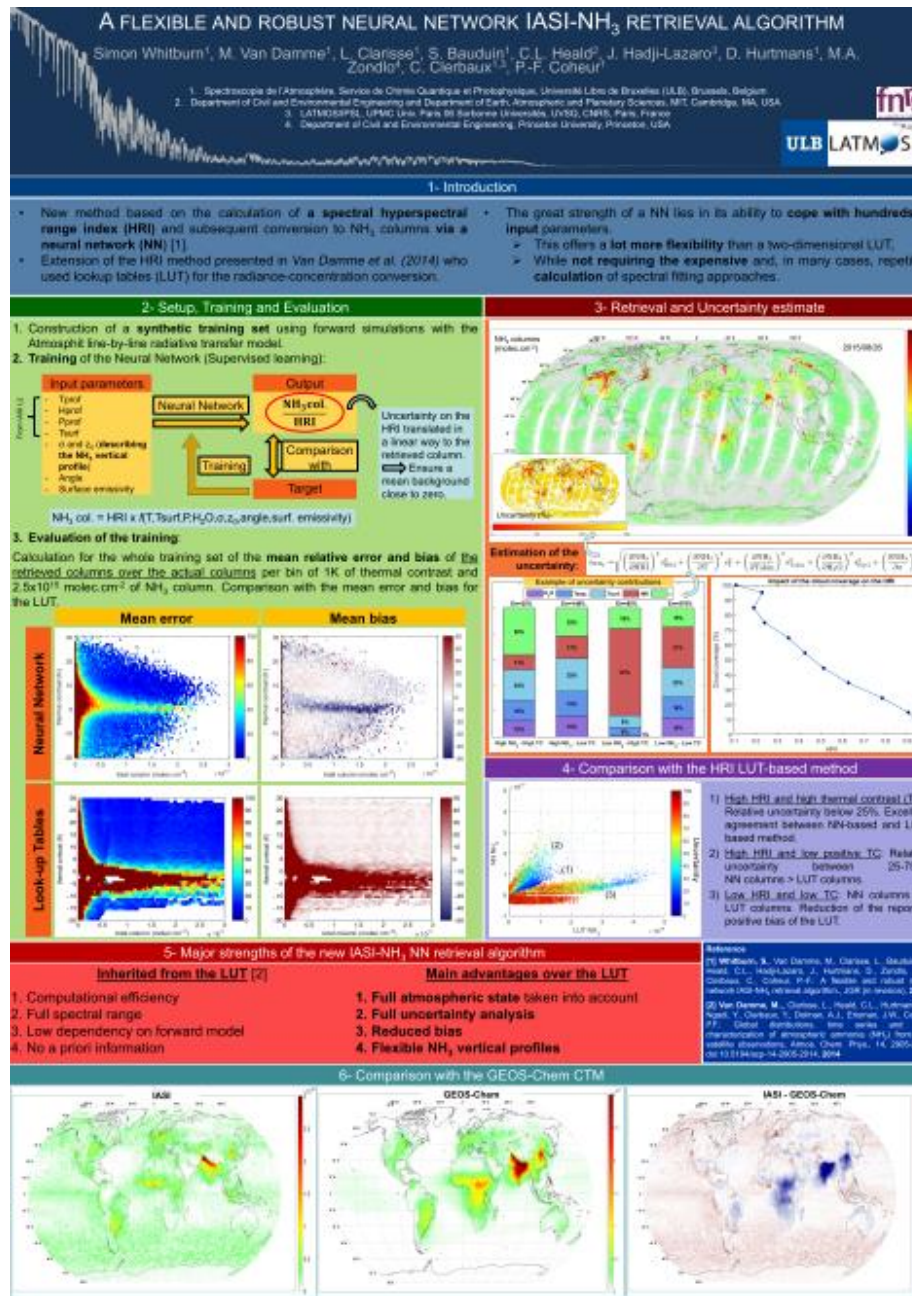
- Fast
- Full spectral range (highly sensitive)
- Low dependency on the forward model (RI, emissivity, etc,)
- Full atmospheric state
- Full uncertainty analysis (propagation of input parameters)

Current limitations

- No retrieval of altitude
- Cloud free conditions

First evaluations

- Correlations with AERONET $> \sim 0.8$
- Comparison with model ‘satisfactory’ (qualitatively)
- Continuity: Land/Ocean – AM/PM



A flexible and robust IASI-NH₃ retrieval algorithm

S. Whitburn, M. Van Damme, L. Clarisse, C. Heald,
C. Clerbaux, D. Hurtmans & P.-F. Coheur

October 26, 2015

In recent years, infrared sounders on board satellites have demonstrated their capabilities to detect and measure ammonia (NH₃) in the atmosphere. The retrieval of NH₃ total columns from satellite-based measurements is, however, still challenging due to variable accuracy of the measurements. In this paper, we describe a new flexible and robust NH₃ retrieval algorithm from the measurements of the Infrared Atmospheric Sounding Interferometer (IASI). The method is an extension of the method developed recently by [2]. The scheme is still based on the calculation of a spectral index (HRI) from the level1C radiances, but instead of using two-dimensional look-up tables (LUT) built from forward radiative transfer model simulations for the conversion of HRI to NH₃ columns, it relies on a neural network (NN) for the conversion. The NN-based HRI method combines the advantages of the LUT-based method whilst providing several significant improvements, including (1) a reduction of the residual dependences by the use of full atmospheric states as input in the neural network, (2) the possible use of flexible NH₃ vertical profiles, and (3) the absence of significant positive bias on the measurement owing to the parametrization of the neural network. The retrieval also includes a full uncertainties analysis of the retrieved columns. We retrieve the NH₃ total columns for the year 2013 and we derive global distributions following arithmetic and weighted averaging procedures. We observe the same main hotspots that were already identified in [2]. We also emphasize the absence of significant positive bias in the average NH₃ distributions. We next give a first assessment of the impact of the NH₃ vertical profile on the retrieved column on a global scale by considering the planetary boundary layer height provided by the ERA-interim re-analysis produced by the ECMWF as value for the thickness of the NH₃ layer.

1 Introduction

Ammonia (NH₃) is released in the atmosphere primarily by agricultural activities and biomass burning. It has a serious impact on air quality and human health as a precursor of secondary aerosols, and leads to acidification and eutrophication of ecosystems. We refer the reader to [2] and references therein for a review on the biogeochemical impacts of NH₃, and its role in the global nitrogen cycle.

Our present knowledge on atmospheric ammonia levels comes from a combination of in-situ measurements, emission inventories coupled with models and from satellite measurements. In-situ measurements (e.g. [7]) are useful on local scales and can give insight into emission sources and the different atmospheric processes at play. However, because of the highly reactive nature of NH₃ and thus its short lifetime they contribute only indirectly to our knowledge of the global spatio-temporal variability of NH₃. Emission inventories, based on e.g. livestock and fire counts coupled with global transport models, were until recently the only way of estimating the global distribution. Current uncertainties on local, but also global emissions remain very large, even when averaged over longer time periods [2].

The newfound possibility of measuring ammonia with infrared satellite sounders has allowed measuring ammonia on a daily global basis. Since the first satellite observations of ammonia were reported, continuous improvements have been made to the retrieval algorithms, increasing both sensitivity and accuracy. The potential of such measurements to improve our understanding and knowledge of emission sources, sinks and transport pathways through comparison and assimilation

